NeuroImage 200 (2019) 621–634

Contents lists available at ScienceDirect

NeuroImage

journal homepage: www.elsevier.com/locate/neuroimage

Detailed mapping of human habenula resting-state functional connectivity

Benjamin A. Ely [a,b,*], Emily R. Stern [c,d], Joo-won Kim [b,e,f], Vilma Gabbay [a,d,g], Junqian Xu [a,b,e,f,1,**]

[a] Department of Neuroscience, Icahn School of Medicine at Mount Sinai, New York, NY, USA
[b] Graduate School of Biomedical Sciences, Icahn School of Medicine at Mount Sinai, New York, NY, USA
[c] Department of Psychiatry, New York University Langone School of Medicine, New York, NY, USA
[d] Nathan S. Kline Institute for Psychiatric Research, Orangeburg, NY, USA
[e] Translational and Molecular Imaging Institute, Icahn School of Medicine at Mount Sinai, New York, NY, USA
[f] Department of Radiology, Icahn School of Medicine at Mount Sinai, New York, NY, USA
[g] Department of Psychiatry, Icahn School of Medicine at Mount Sinai, New York, NY, USA

ARTICLE INFO

Keywords:
fMRI
Reward
Salience
Pain
Sensory cortex
Default mode network

ABSTRACT

The habenula (Hb) inhibits dopaminergic reward signaling in response to negative outcomes and has been linked to numerous functional domains relevant to mental health, including reward prediction, motivation, and aversion processing. Despite its important neuroscientific and clinical implications, however, the human Hb remains poorly understood due to its small size and the associated technical hurdles to *in vivo* functional magnetic resonance imaging (fMRI) investigation. Using high-resolution 3 T fMRI data from 68 healthy young adults acquired through the Human Connectome Project, we developed a rigorous approach for mapping the whole-brain resting-state functional connectivity of the human Hb. Our study combined an optimized strategy for defining subject-level connectivity seeds to maximize Hb blood-oxygen-level-dependent (BOLD) signal sensitivity with high-quality surface-based alignment for robust functional localization and cortical sensitivity. We identified significant positive Hb connectivity with: (i) conserved brainstem targets, including the dopaminergic ventral tegmental area, serotonergic raphe nuclei, and periaqueductal gray; (ii) subcortical structures related to reward and motor function, including the nucleus accumbens, dorsal striatum, pallidum, thalamus, and cerebellum; and (iii) cortical areas associated with the Salience Network and early sensory processing, including the dorsal anterior cingulate, anterior insula, and primary visual and auditory cortices. Hb connectivity was strongly biased towards task-positive brain regions, with weak or negative connectivity observed throughout the task-negative Default Mode Network. Our study provides a detailed characterization of Hb resting-state functional connectivity in healthy young adults, demonstrating both the feasibility and clinical potential of studying the human Hb using high-resolution 3 T fMRI.

1. Introduction

The habenula (Hb), a small pair of highly conserved nuclei bordering the dorsomedial thalamus, is thought to play a key role in reward inhibition, motivation, and aversion processing (Matsumoto and Hikosaka, 2007; Fore et al., 2018). The Hb is divided into functionally and

Abbreviations: ACC, Anterior Cingulate Cortex; BOLD, Blood-Oxygen-Level-Dependent; CM, Centromedian; CSF, Cerebrospinal Fluid; dlPFC, Dorsolateral Prefrontal Cortex; dmPFC, Dorsomedial Prefrontal Cortex; DM, Dorsomedial; FEF, Frontal Eye Fields; FWE, Familywise Errors; FWHM, Full Width at Half Maximum; Hb, Habenula; HCP, Human Connectome Project; MGR, Mean Gray Matter Timeseries Regression; MSM, Multimodal Surface Matching; NAc, Nucleus Accumbens; OFC, Orbital Frontal Cortex; PAG, Periaqueductal Gray; PCA, Principle Component Analysis; PET, Positron Emission Tomography; RMTg, Rostromedial Tegmental Nucleus; ROI, Region of Interest; rs-fMRI, Resting-State Functional Magnetic Resonance Imaging; SMA, Supplementary Motor Area; SN, Substantia Nigra; SNR, Signal-to-Noise Ratio; TFCE, Threshold-Free Cluster Enhancement; TPJ, Temporoparietal Junction; TS, Timeseries; vmPFC, Ventromedial Prefrontal Cortex; VTA, Ventral Tegmental Area; WM, White Matter.

* Corresponding author. Icahn School of Medicine at Mount Sinai, One Gustave L. Levy Place, Box 1234, New York, NY, USA.
** Corresponding author. Icahn School of Medicine at Mount Sinai, One Gustave L. Levy Place, Box 1234, New York, NY, USA.
E-mail addresses: benjamin.ely@mssm.edu (B.A. Ely), junqian.xu@mssm.edu (J. Xu).
[1] Current affiliation: This author is now affiliated with Baylor College of Medicine, Houston, TX, USA.

https://doi.org/10.1016/j.neuroimage.2019.06.015
Received 9 March 2019; Received in revised form 15 May 2019; Accepted 4 June 2019
Available online 25 June 2019

cytologically distinct medial and lateral nuclei and forms the centerpiece of the "dorsal diencephalic conduction system", a major link between midbrain monoamine nuclei, the basal ganglia, and limbic areas (Sutherland, 1982). The medial Hb primarily projects to the interpeduncular nucleus and receives the majority of its inputs from the septum (Herkenham and Nauta, 1977). The synaptic profile of the lateral Hb is more complex, innervating targets throughout the midbrain and brainstem including the dopaminergic ventral tegmental area (VTA) and substantia nigra (SN) pars compacta, serotonergic dorsal and median raphe nuclei, and periaqueductal gray (PAG) (Herkenham and Nauta, 1979; Quina et al., 2015; Zahm and Root, 2017). Major inputs to the lateral Hb include the hypothalamus, pallidum, and reciprocal projections from midbrain and brainstem nuclei (Herkenham and Nauta, 1977; Zahm and Root, 2017). Due to its influence over monoamine signaling and involvement in many functional domains related to reward and motivation, human Hb circuitry may have important clinical implications (Boulos et al., 2017).

Lateral Hb inhibition of dopaminergic reward signaling in response to negative reward prediction errors (i.e., absence of expected rewards) and aversive stimuli has been particularly well characterized in animal models (Stamatakis and Stuber, 2012; Boulos et al., 2017), including nonhuman primates (Matsumoto and Hikosaka, 2007; Kawai et al., 2015). In rodents, optogenetic stimulation of lateral Hb neurons results in behavioral avoidance, reduced motivation to obtain rewards, and other depressive phenotypes (Stamatakis and Stuber, 2012; Proulx et al., 2018). Conversely, lateral Hb inhibition or lesions ameliorate a range of depression-like behaviors (Li et al., 2016; Proulx et al., 2018) but trigger increased impulsivity and reward seeking, phenotypes associated with addiction (Stamatakis et al., 2016; Zapata et al., 2017). Moreover, recent evidence suggests that the rapid antidepressant effects of ketamine are driven by its action at the lateral Hb (Yang et al., 2018). However, while an abundance of studies have now described normative and aberrant Hb function in animals, efforts to translate these findings to human research have proceeded slowly (Boulos et al., 2017).

Roadblocks to understanding the human Hb primarily stem from methodological limitations. Characterizing Hb function *in vivo* is technically challenging due to the structure's small size, reported as 30–40 mm^3 per hemisphere in postmortem histology (Ahumada-Galleguillos et al., 2017), which is comparable to the volume of a single voxel (i.e., $\geq 27\ mm^3$) in conventional 3 T functional magnetic resonance imaging (fMRI) studies with whole-brain coverage. Consequently, although task fMRI studies at conventional resolution have occasionally reported activation in the vicinity of the Hb following negative outcomes, including reward prediction errors (Salas et al., 2010) and acute pain (Shelton et al., 2012b), these results likely represent a mixture of signals from the Hb and nearby structures (e.g., dorsomedial thalamic nuclei). Recent efforts to localize human Hb activity more accurately have largely focused on acquiring higher resolution fMRI data (i.e., $\leq 8\ mm^3$ per voxel). In line with earlier results, these high-resolution task fMRI studies have documented Hb activation in response to cues predicting aversive outcomes in healthy adults (Lawson et al., 2014; Hennigan et al., 2015), a pattern that was disrupted in depressed adults (Lawson et al., 2017). Unfortunately, almost all high-resolution Hb fMRI studies have been performed with limited brain coverage, excluding large portions of the cortex and, in some cases, subcortex. Moreover, previous Hb fMRI studies have only been performed using traditional 3D volume-based analysis methods. Although this approach works well for subcortical gray matter, which is largely composed of globular nuclei, it does not accurately represent the neuroanatomy of cortical gray matter as a thin, highly convoluted sheet. Modeling cortical fMRI data instead using 2D surface-based analysis significantly improves sensitivity, inter-subject alignment, and ability to localize signals (Coalson et al., 2018). As a result, the details of human Hb-cortical interactions remain particularly poorly characterized.

Human Hb circuitry also remains critically underexplored using resting-state fMRI (rs-fMRI). Unlike task fMRI, which measures changes in blood-oxygen-level-dependent (BOLD) signals to infer regional activation or deactivation in response to specific stimuli, rs-fMRI measures spontaneous BOLD signal fluctuations during undirected rest, providing unique information about the intrinsic organization of brain activity (Fox and Raichle, 2007). Correlations in low-frequency rs-fMRI signals (i.e., resting-state functional connectivity) reflect a combination of direct anatomical links between regions as well as indirect, polysynaptic circuits, and are agnostic to the direction of information flow between regions; functional connectivity is often, but not always, stronger between areas with more extensive anatomical connections (Honey et al., 2009). Only three high-resolution Hb rs-fMRI studies have been published to date: two by other groups with partial brain coverage at 3 T (Hétu et al., 2016) and 7 T (Torrisi et al., 2017), and one by our group using whole-brain 3 T data but a cohort comprised of only subjects with high or low levels of subclinical depression (Ely et al., 2016). These initial rs-fMRI studies are informative, independently reporting positive Hb connectivity with key reward-related areas such as the VTA and dorsal anterior cingulate cortex (ACC), but lack consensus regarding Hb connectivity with important aversion-related regions (e.g., PAG, insula). The need therefore remains for a detailed, neurobiologically accurate map of Hb connectivity in healthy adults.

In the current study, we examined whole-brain Hb resting-state functional connectivity in a representative sample of 68 healthy young adults from the Human Connectome Project (HCP) (Van Essen et al., 2013), which uses recent advances in multiband acceleration to achieve whole-brain fMRI coverage with high spatial and temporal resolution (Smith et al., 2013). Analyses were performed in CIFTI grayordinate space, which represents the subcortex as a 3D volume and the cortex as a pair of left and right 2D surfaces to accurately reflect the distinct neuroanatomy of these regions (Glasser et al., 2013; Coalson et al., 2018), and included multimodal surface matching (MSM) for robust inter-subject cortical alignment and functional localization (Robinson et al., 2014; Glasser et al., 2016a). To maximize Hb BOLD sensitivity, we evaluated six ways to generate Hb regions of interest (ROIs) at functional resolution for use as connectivity seeds. Secondary analyses described in the Supplementary Materials further assessed the impact of common methodological variations on Hb connectivity results. Our goal for this study was to provide a comprehensive, benchmark description of human Hb resting-state functional connectivity in healthy adults.

2. Materials and methods

See Fig. 1 for a schema of our preprocessing and analysis procedures. Methodology for all secondary analyses is described in the Supplementary Methods (section S1).

2.1. Data acquisition and preprocessing

Subjects comprised 68 healthy young adults (41 female; 8 monozygotic twin pairs; 9 dizygotic twin pairs; age 29.6 ± 3.1 years) from the WU-Minn HCP Consortium (Van Essen et al., 2013), representing all subjects from the HCP 900 Subjects Release with complete anatomical datasets at 3 T and rs-fMRI datasets at both 3 T and 7 T. Five subjects were included in our previous Hb connectivity study (Ely et al., 2016). Data were deidentified by the HCP prior to public release and considered exempt from review by the Mount Sinai Institutional Review Board; participants provided informed consent to the HCP for all imaging and data sharing procedures. Imaging data used for the current study constituted one T1w MPRAGE and one T2w SPACE anatomical scan at 0.7 mm isotropic resolution (Glasser et al., 2013) and four 15 min rs-fMRI scans at 2 mm isotropic resolution with TR/TE = 720/36 ms (Smith et al., 2013), all acquired at 3 T. Anatomical and functional data were visually inspected and minimally preprocessed by HCP prior to release (e.g., distortion corrected, coregistered, warped to MNI and CIFTI grayordinate templates; see Glasser et al., 2013 for full details). Whole-brain connectivity analyses were performed using rs-fMRI data in CIFTI grayordinate

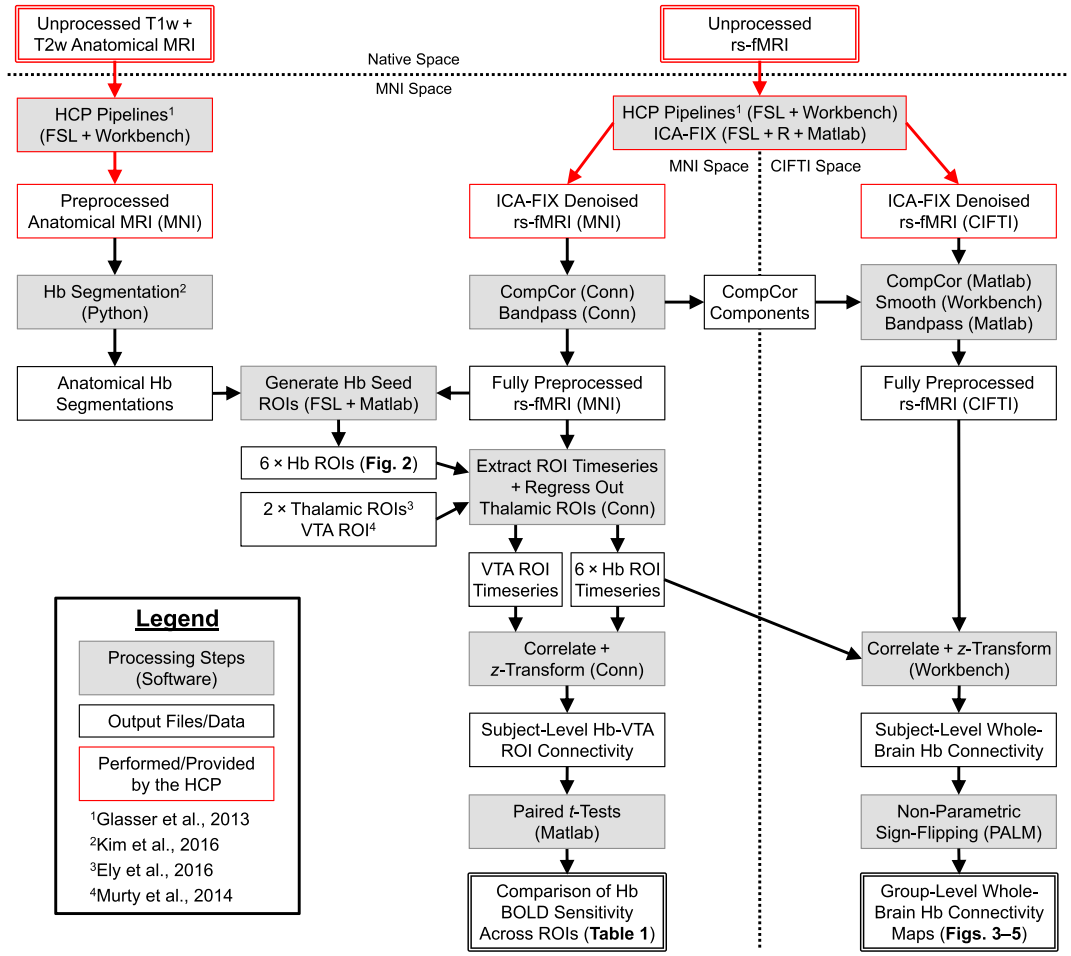

Fig. 1. Overview of preprocessing and analysis procedures. **Top**: Acquisition and initial preprocessing of anatomical MRI and rs-fMRI data by the HCP, including distortion correction, coregistration, standardization to MNI and CIFTI grayordinate template spaces, ICA-FIX denoising of rs-fMRI data, and MSMAll alignment of cortical surface data. **Left**: Subject-level Hb segmentation at 0.7 mm isotropic anatomical resolution in MNI space. Anatomical Hb segmentations and unsmoothed rs-fMRI data were used to generate six types of Hb seed ROIs at 2 mm isotropic functional resolution (see Fig. 2). **Center**: Further preprocessing of rs-fMRI data in MNI space via CompCor denoising (5 WM and 5 CSF components) and bandpass filtering (0.1–0.01 Hz). After regressing out timeseries from two nearby thalamic ROIs, Hb ROIs were evaluated based on connectivity with a template VTA ROI as a proxy for Hb BOLD sensitivity using paired *t*-tests. **Right**: After equivalent preprocessing as well as spatial smoothing (FWHM = 4 mm), rs-fMRI data in CIFTI grayordinate space were correlated with the extracted Hb ROI timeseries to generate whole-brain resting-state functional connectivity maps. Group-level statistics were calculated using non-parametric sign-flipping with 10,000 iterations.

space, which represents the cortex using 2D left and right surface meshes (32 k vertices per surface) and the subcortex using 3D MNI coordinates (2 mm isotropic voxel spacing), while ROI timeseries were extracted from rs-fMRI data in MNI space (see below). MSM was performed by the HCP to identify and align corresponding cortical locations across subjects based on a combination of cortical folding, thickness, myelination, and resting-state functional connectivity features (i.e., MSMAll alignment) (Robinson et al., 2014; Glasser et al., 2016a). The HCP also performed initial denoising of rs-fMRI data using an automated independent components analysis (ICA) classifier, ICA-FIX (Griffanti et al., 2014; Salimi-Khorshidi et al., 2014).

To address remaining structured noise in the rs-fMRI data (Inline Supplementary Fig. S1), we performed principle component analysis (PCA) within subject-level white matter (WM) and cerebrospinal fluid (CSF) masks and regressed out the five largest PCA components from each (i.e., anatomical CompCor denoising) using Conn Toolbox version 17f (Whitfield-Gabrieli and Nieto-Castanon, 2012). Tissue masks were derived from slightly eroded FreeSurfer segmentations provided by the HCP. We next performed spatial smoothing on rs-fMRI data in CIFTI grayordinate space with a 4 mm full width at half maximum (FWHM) Gaussian kernel applied to each cortical surface and the unconstrained subcortical volume using Connectome Workbench version 1.2.3 (Marcus et al., 2011). Importantly, however, all ROI timeseries were extracted from unsmoothed rs-fMRI data in MNI space using Conn. Finally, rs-fMRI data were bandpass filtered (0.1–0.01 Hz), also using Conn.

2.2. Generating habenula regions of interest

We performed subject-level semi-automated Hb segmentation (Kim et al. 2016, 2018) in MNI space at anatomical resolution (i.e., 0.7 mm isotropic) using T1w, T2w, and T1w/T2w ratio images (threshold factor $\alpha = 0.8$; see Kim et al., 2016). This yielded left and right: (i) probabilistic Hb segmentations, where the weight of each voxel represented the fraction of that voxel composed of Hb tissue (red in Fig. 2); (ii) binary Hb segmentations, which included all voxels containing predominantly Hb tissue; and (iii) total volume estimates, which were based on the weighted sum of voxels in the probabilistic Hb segmentations. As illustrated in Fig. 2, we then generated Hb ROIs at functional resolution (i.e., 2 mm isotropic) for use as functional connectivity seeds using six distinct methods:

1) *Unoptimized* ROIs: Conservatively defined ROIs created by downsampling subjects' binary Hb segmentations to functional resolution using linear registration with nearest-neighbour interpolation, as implemented in FSL version 5.0.6 (Jenkinson et al., 2002).

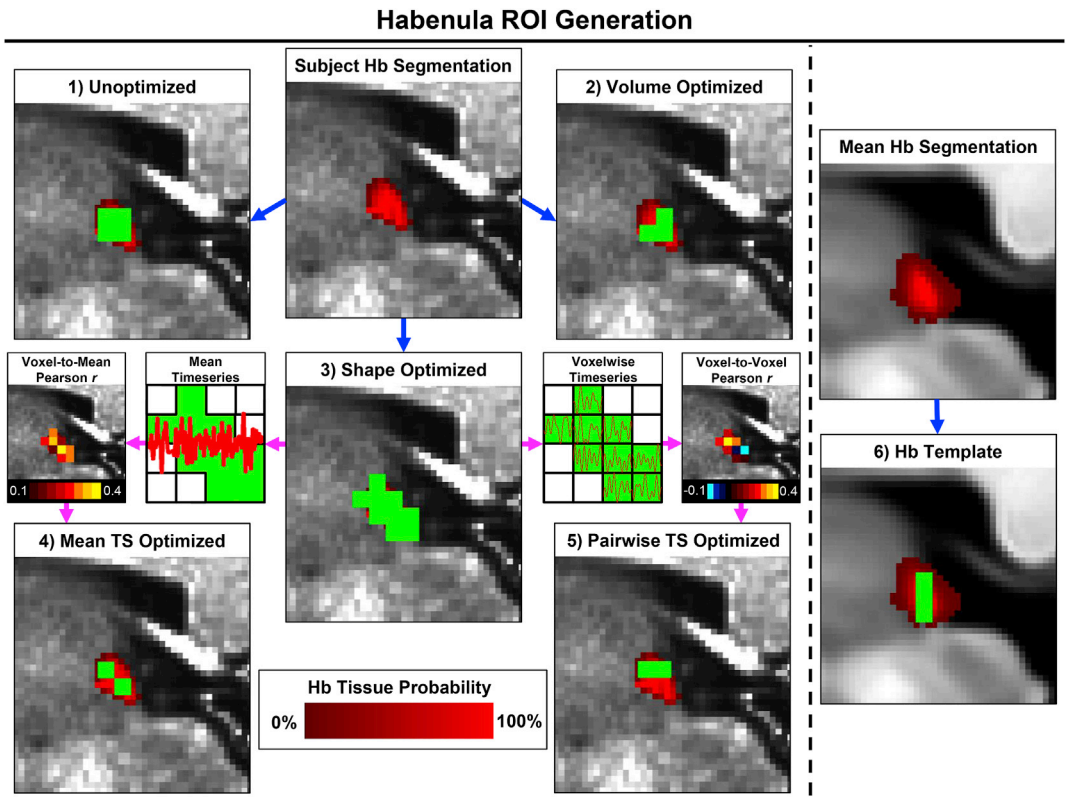

Fig. 2. Creation of subject-level Hb ROIs in a representative subject (**panels 1**–**5**) and of the group-level *Hb Template* ROI (**panel 6**). Hb ROIs at 2 mm functional resolution (green) are overlaid on probabilistic anatomical Hb segmentations at 0.7 mm anatomical resolution (red). Blue arrows indicate ROIs derived solely from anatomical Hb segmentations. Magenta arrows indicate ROIs derived from both anatomical segmentations and rs-fMRI data (illustrated in subpanels). Note that *Volume Optimized* (**panel 2**), *Mean Timeseries (TS) Optimized* (**panel 4**), and *Pairwise Timeseries (TS) Optimized* (**panel 5**) ROIs contained the same number of voxels, not all of which can be seen in the single slice presented.

2) *Volume Optimized* ROIs: Similar to *Unoptimized* ROIs, but based on subjects' probabilistic Hb segmentations. Tissue probability thresholds were individually adjusted before downsampling such that the volume of each *Volume Optimized* ROI matched the corresponding individual Hb volume estimate, minimizing changes in size due to interpolation. This was the method used in our previous Hb connectivity study (Ely et al., 2016).
3) *Shape Optimized* ROIs: Empirically designed to approximate the shape and outer boundaries of subjects' anatomical Hb segmentations. Generated by thresholding probabilistic Hb segmentations at 25% tissue probability, then identifying and combining all fMRI voxels with coordinates that overlapped with at least four anatomical voxels from the thresholded Hb segmentation. *Shape Optimized* ROIs also served as the "search space" of voxels used to create *Mean Timeseries Optimized* and *Pairwise Timeseries Optimized* ROIs.
4) *Mean Timeseries Optimized* ROIs: Voxels within the *Shape Optimized* ROI most strongly correlated with the mean timeseries of the bilateral *Shape Optimized* ROI. *Mean Timeseries Optimized* ROI volumes were matched to estimated Hb volumes, as in *Volume Optimized* ROIs.
5) *Pairwise Timeseries Optimized* ROIs: Voxels within the *Shape Optimized* ROI that had the strongest pairwise (i.e., single voxel to single voxel) timeseries correlations. *Pairwise Timeseries Optimized* ROI volumes were matched to estimated Hb volumes, as in *Volume Optimized* ROIs.
6) *Hb Template* ROI: A generic (i.e., not individual-specific) ROI created by averaging all subjects' probabilistic Hb segmentations to create a mean Hb segmentation. This was then thresholded before downsampling such that the *Hb Template* ROI matched the average segmented Hb volume estimate, similar to the subject-level thresholding used to create *Volume Optimized* ROIs.

ROIs were created separately in the left and right hemisphere and then combined to obtain bilateral connectivity seeds. Scripts to generate all Hb ROI types from input Hb segmentations are available at https://github.com/junqianxulab/Habenula_fMRI_ROIs.

2.3. Evaluating habenula regions of interest

Hb ROIs were primarily evaluated based on connectivity with the VTA (Fig. 1, center), which we used as a proxy for Hb BOLD sensitivity. A template VTA ROI was created by empirically thresholding a publicly available probabilistic VTA atlas (Murty et al., 2014) at 75% tissue probability and binarizing. Hb ROI timeseries were separately extracted for each run from unsmoothed but otherwise fully preprocessed rs-fMRI data in MNI space. Subject-level Hb-VTA ROI connectivity was calculated using version 17f of the Conn Toolbox (Whitfield-Gabrieli and Nieto-Castanon, 2012) as the Fisher *z*-transformed semi-partial correlation between each Hb timeseries and the VTA timeseries, controlled for two nearby thalamic ROIs approximately corresponding to the dorsomedial (DM) and centromedian (CM) nuclei (Ely et al., 2016). Subject-level timeseries correlations were calculated separately for each run and then averaged across the four rs-fMRI runs. Hb-VTA connectivity was compared across the six Hb ROI types at the group level using paired *t*-tests, with differences considered significant at the two-tailed, Bonferroni-corrected $p_{critical} < 0.0083$ (i.e., 0.05/6).

2.4. Whole-brain habenula functional connectivity analysis

After regressing out the two thalamic ROI timeseries, extracted Hb timeseries values were correlated with the timeseries of each cortical surface vertex and subcortical voxel in 32 k CIFTI grayordinate space (i.e., 91,282 total correlations) using Connectome Workbench (Fig. 1, right). Results from the four rs-fMRI runs were Fisher *z*-transformed and

averaged to yield final subject-level connectivity maps. Group-level connectivity statistics were computed using nonparametric sign-flipping (10,000 iterations) and corrected for familywise errors (FWE) using threshold-free cluster enhancement (TFCE), as implemented in FSL PALM version alpha111 (Winkler et al., 2014), with results considered significant at the $p_{TFCE\text{-}FWE} < 0.05$ threshold. Exchangeability blocks were used to control for family structure (Winkler et al., 2015). Since arbitrary statistical thresholds can obscure meaningful patterns in underlying fMRI data (e.g., rapid changes in connectivity across boundaries between cortical areas) (Glasser et al., 2016b), unthresholded Hb connectivity maps were also examined.

3. Results

3.1. Habenula region of interest evaluation

All six Hb ROI types showed very significant functional connectivity ($p < 10^{-5}$) with the VTA ROI (Table 1). However, paired *t*-tests revealed that *Shape Optimized* ROIs had significantly stronger VTA connectivity than any other Hb ROI type (all $p < 10^{-3}$), and were also the only Hb ROI type with significantly stronger VTA connectivity than the two nearby thalamic ROIs (both $p < 2 \times 10^{-3}$).

Whole-brain analyses indicated that *Shape Optimized* ROIs also had the strongest connectivity with many other brain areas (Fig. 3), including the dorsal ACC, mid-cingulate, and insula. Whole-brain connectivity patterns were highly consistent across the six Hb ROI types, particularly without statistical thresholding (Fig. 3, left), suggesting that the connectivity differences seen at the $p_{TFCE\text{-}FWE} < 0.05$ level (Fig. 3, right) likely reflect the arbitrary nature of the chosen significance threshold rather than intrinsic neurobiological differences. Thus, of the six Hb ROI types we evaluated, *Shape Optimized* ROIs had the best sensitivity to Hb BOLD signals and comparable specificity, despite being substantially larger than the other ROI types (see section S2.1 of Supplementary Results). Cortical connectivity with *Shape Optimized* Hb ROIs also closely followed multimodal areal boundaries defined by the HCP (Fig. 5A), further suggesting that these ROIs captured coherent underlying neural signals. Detailed results and figures are therefore based on *Shape Optimized* Hb ROIs except where noted.

3.2. Habenula functional connectivity overview

Detailed whole-brain resting-state functional connectivity results using *Shape Optimized* Hb ROIs are presented in Fig. 4. Significant positive connectivity between the Hb and cortex (Fig. 4A–D) was most pronounced with midline cingulate structures, particularly the dorsal ACC, mid-cingulate, and retrosplenial cingulate, as well as the insula (Fig. 4R), dorsolateral prefrontal cortex (dlPFC), and early sensory/motor regions. Positive connectivity between the Hb and subcortical areas (Fig. 4E–K) was widespread but particularly prominent with the thalamus and midbrain, including peaks in the VTA, raphe nuclei, and PAG (Fig. 4L–Q). Negative Hb connectivity met significance for only a few regions of the lateral temporal and occipital lobes in the main analysis (Fig. 4A,D). Secondary analyses presented in the Supplementary Results (section S2) explored the impact of different methodological choices on Hb connectivity: using separate left or right rather than bilateral Hb seeds (Inline Supplementary Fig. S2); performing mean gray matter timeseries regression (MGR) to remove global fMRI signal effects (Inline Supplementary Fig. S3); using unsmoothed rs-fMRI data (Inline Supplementary Fig. S4); and performing a "parcellated" connectivity analysis (Inline Supplementary Fig. S5 and Inline Supplementary Table S1) by averaging rs-fMRI timeseries within 206 bilateral cortical and subcortical regions, adapted from the multimodal cortical parcellation recently released by the HCP (Glasser et al., 2016a). Cortical area labels used in this study also follow the multimodal HCP parcellation, which maintains established naming conventions where possible (e.g., "area d32" = dorsal portion of Brodmann area 32). Connectivity maps and related data from all analyses are freely available for download from the BALSA database (Van Essen et al., 2017) at https://balsa.wustl.edu/study/show/3ggmZ.

Hb connectivity findings below are presented separately for specific brain structures (section 3.3) and distributed brain networks (section 3.4).

3.3. Habenula connectivity with specific structures

3.3.1. Ventral tegmental area and substantia nigra

Hb connectivity demonstrated clear selectivity for the VTA within the midbrain (Fig. 4E,H). Although significant Hb connectivity (red-orange) extended to much of the surrounding tissue, including the dopaminergic SN, connectivity was strongest (yellow) at the anterior medial surface of the midbrain, corresponding very well with both the location and shape of the VTA (Mai and Paxinos, 2012; Murty et al., 2014). Even in a secondary analysis performed without spatial smoothing, voxelwise Hb-VTA connectivity still survived FWE correction (Fig. 4P–Q and Inline Supplementary Fig. S4), indicating a high innate BOLD contrast-to-noise ratio. Moreover, our evaluation of Hb seed ROIs found highly

Table 1
Comparison of VTA Connectivity Across Habenula Seed ROIs.

ROI Type	VTA Connectivity[a]		Paired *t*-Tests (two-tailed *p* values)[c]						
	t	r^b	*Unoptimized*	*Volume Optimized*	*Shape Optimized*	*Mean TS Optimized*	*Pairwise TS Optimized*	*Hb Template*	*DM Thalamus*
Unoptimized	4.8	0.024 ± 0.042	—	—	—	—	—	—	—
Volume Optimized	7.4	0.037 ± 0.041	1.4×10^{-3}	—	—	—	—	—	—
Shape Optimized	10.8	0.058 ± 0.044	**5.3×10^{-11}**	**9.1×10^{-7}**	—	—	—	—	—
Mean TS Optimized	6.7	0.034 ± 0.041	0.054	0.49	**1.3×10^{-7}**	—	—	—	—
Pairwise TS Optimized	6.5	0.036 ± 0.046	0.029	0.88	1.5×10^{-5}	0.55	—	—	—
Hb Template	8.4	0.044 ± 0.043	4.5×10^{-5}	0.11	9.4×10^{-4}	0.028	0.14	—	—
DM Thalamus	6.7	0.038 ± 0.046	0.080	> 0.99	1.7×10^{-3}	0.72	0.94	0.24	—
CM Thalamus	2.9	0.013 ± 0.037	0.086	4.8×10^{-4}	**1.3×10^{-8}**	1.9×10^{-3}	1.6×10^{-3}	2.9×10^{-5}	2.8×10^{-4}

[a]Group-level VTA connectivity was highly significant ($p < 10^{-5}$) for all Hb ROIs.
[b]Semi-partial Pearson correlations (mean ± standard deviation). Hb ROI connectivity controlled for the two thalamic ROI timeseries. Thalamic ROI connectivity controlled for the other thalamic ROI and *Unoptimized* Hb ROI timeseries.
[c]Bonferroni-adjusted $p_{critical} = 0.05/6 \approx 8.3 \times 10^{-3}$ for Hb ROIs. Highly significant results ($p < 10^{-5}$) displayed in **bold**. Nonsignificant results displayed in gray.

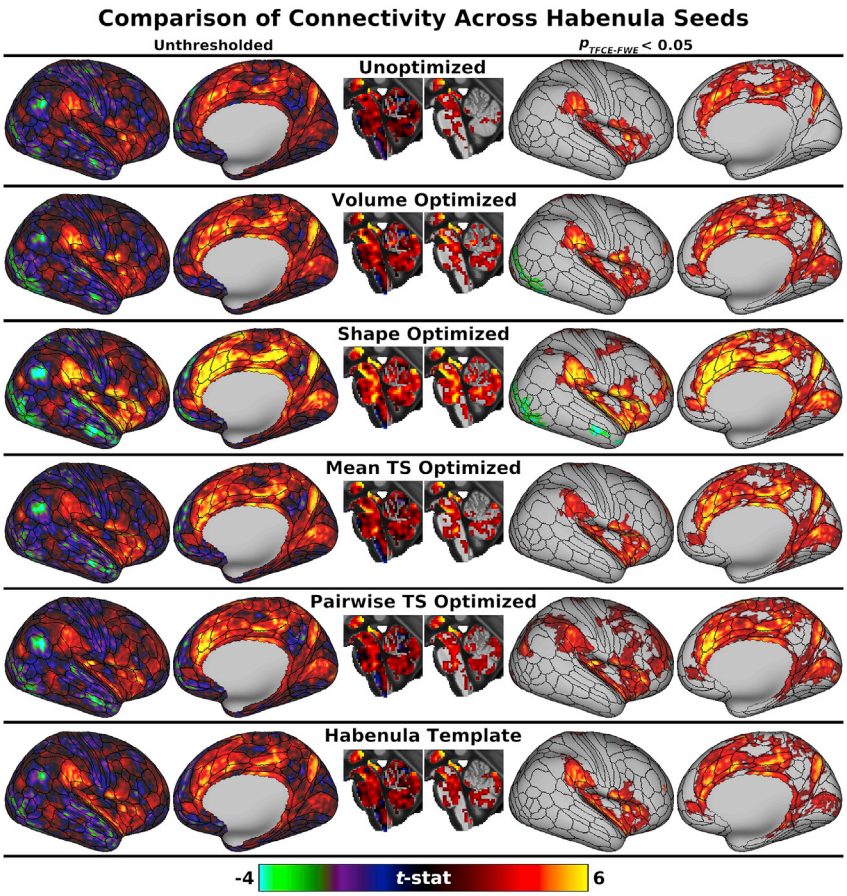

Fig. 3. Unthresholded (**left**) and significance-thresholded ($p_{TFCE\text{-}FWE} < 0.05$, **right**) whole-brain connectivity results for the six types of Hb seed ROIs (see Fig. 2), displayed on the "very inflated" right cortical surface with areal boundary lines from the multimodal HCP parcellation (Glasser et al., 2016a) and a midsagittal slice through subcortical MNI space (X = 0). Unthresholded connectivity patterns were largely consistent across Hb seeds, including positive connectivity with the dorsal ACC, mid-cingulate, insula, posterior precuneus, and VTA. However, strength of connectivity with these areas varied between Hb seeds, resulting in larger apparent differences after significance thresholding (e.g., primary visual cortex and dlPFC). Connectivity was generally strongest for *Shape Optimized* ROIs and weakest for *Unoptimized* ROIs. Left hemisphere results (not presented) were very similar.

significant connectivity ($t = 10.8$, $r = 0.058 \pm 0.044$) between the *Shape Optimized* ROIs used in our main analysis and the template VTA ROI (Table 1); significance and correlation strength (mean ± standard deviation) were fairly consistent across run 1 ($t = 5.2$, $r = 0.053 \pm 0.084$), run 2 ($t = 5.7$, $r = 0.068 \pm 0.098$), run 3 ($t = 4.0$, $r = 0.043 \pm 0.089$), and run 4 ($t = 6.3$, $r = 0.063 \pm 0.082$).

3.3.2. *Raphe nuclei*

As shown in Fig. 4L–O, Hb connectivity peaks along the medial brainstem closely corresponded to the locations of human dorsal, median, and magnus raphe nuclei (Mai and Paxinos, 2012; Son et al., 2012).

3.3.3. *Periaqueductal gray*

Hb connectivity with the PAG was both strong and selective (Fig. 4E,I), with a clear peak (yellow) surrounding the cerebral aqueduct in the main analysis. As with the VTA, voxelwise Hb-PAG connectivity survived FWE correction even in a secondary analysis without spatial smoothing (Fig. 4P and Inline Supplementary Fig. S4).

3.3.4. *Striatum*

Voxelwise Hb connectivity was most pronounced with the putamen, forming two clusters with distinct peaks in the anterior and posterior putamen (Fig. 4I–K) that extended into the pallidum (Fig. 4J). Similarly, Hb connectivity with the caudate centered around two main peaks, one in the dorsal caudate body (Fig. 4F) and another in the ventral caudate head extending into the nucleus accumbens (NAc) (Fig. 4I–K). In the secondary parcellated analysis (Inline Supplementary Fig. S5 and Inline Supplementary Table S1), Hb-striatal connectivity was strongest with the mean timeseries of the putamen ($t = 8.8$) and caudate ($t = 8.1$), but also significant for the pallidum ($t = 4.3$) and NAc ($t = 4.0$).

3.3.5. *Thalamus*

Thalamic Hb connectivity peaks (Fig. 4F,J–K) included a large, bilateral region located superior and anterior to the Hb, which we identified as the dorsomedial and centrolateral thalamic nuclei based on an MNI-standardized stereotactic atlas (Krauth et al., 2010; Jakab et al., 2012). From there, peak Hb connectivity extended laterally to encompass the ventrolateral, ventral posterior lateral, and lateral posterior nuclei. Strong connectivity was also seen with portions of the dorsomedial, centrolateral, limitans, and medial pulvinar nuclei immediately surrounding the Hb; however, these likely reflected the effects of spatial smoothing (FWHM = 4 mm) rather than neurobiologically meaningful connections. Consistent with this interpretation, connectivity with thalamic voxels near the Hb was dramatically reduced in a secondary analysis using unsmoothed fMRI data, whereas other thalamic connectivity peaks remained largely intact (Inline Supplementary Fig. S4). The extremely strong mean Hb-thalamus connectivity ($t = 24.5$) seen in the secondary parcellated analysis (Inline Supplementary Fig. S5 and Inline Supplementary Table S1) was presumably also inflated by the presence of Hb voxels within the thalamus parcel.

3.3.6. *Cerebellum*

Like the thalamus, significant positive Hb connectivity was observed with large portions of the cerebellum (Fig. 4E–H). Connectivity was strongest with cerebellar lobules VI, VIIb, X, vermis VI, and anterior parts of crus I. A secondary analysis using unihemispheric Hb seeds (Inline Supplementary Fig. S2) also found significant negative connectivity between the right Hb and posterior portions of lobules crus I and crus II; this was the only subcortical area to significantly differ in connectivity between left and right Hb seeds.

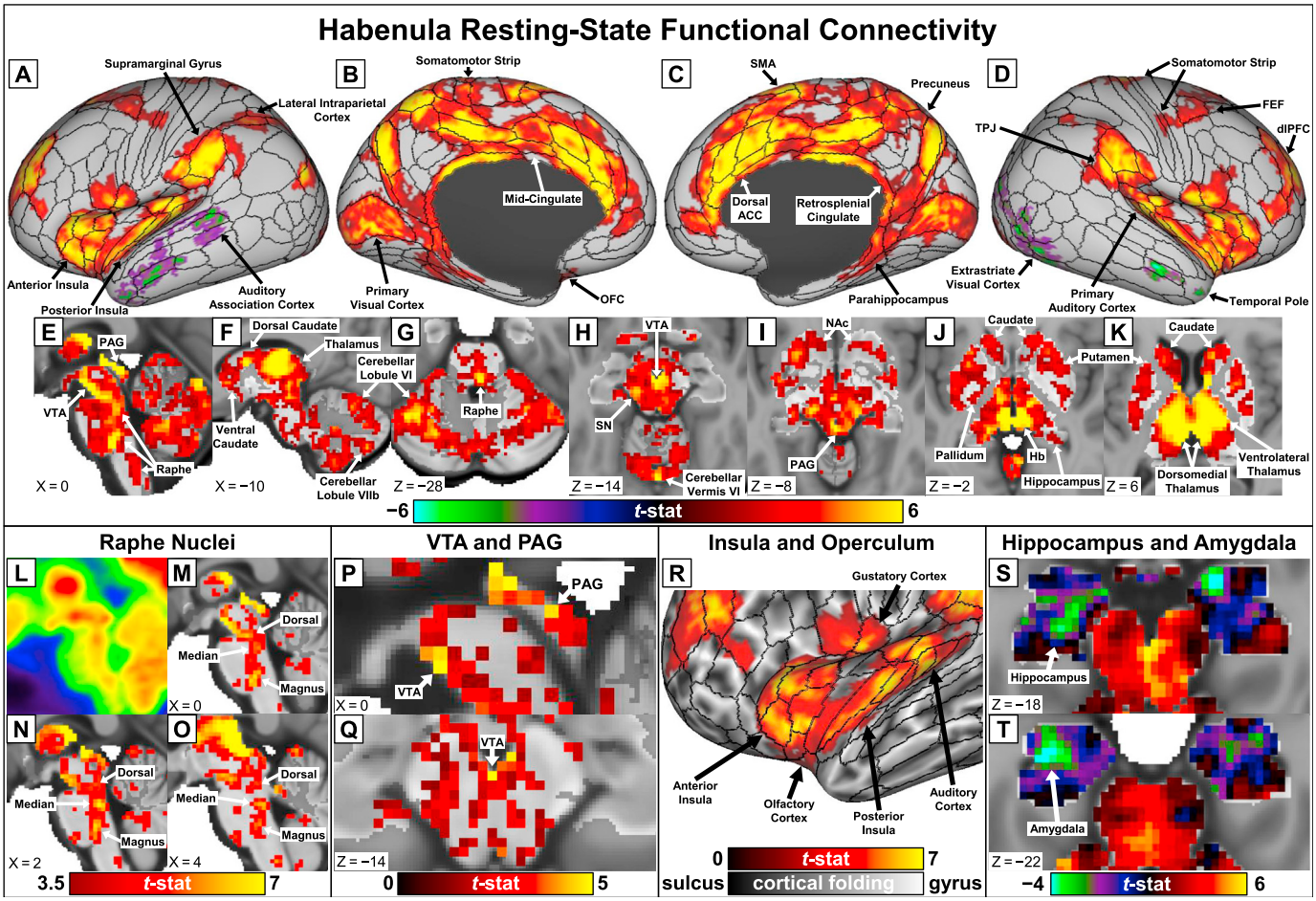

Fig. 4. Whole-brain Hb resting-state functional connectivity results and expanded views of key findings, displayed on "very inflated" cortical surfaces with areal boundary lines from the multimodal HCP parcellation (Glasser et al., 2016a) and in subcortical MNI space. **A**—**K**: Hb connectivity maps for significant ($p_{TFCE\text{-}FWE} < 0.05$) findings in the main analysis. **L**: Midsagittal view of the brainstem showing locations of human raphe nuclei as peaks in mean [^{18}F]fluorodeoxyglucose PET images acquired from seven healthy adults, displayed in MNI space. Reprinted with permission from Son et al. (2012). **M**—**O**: Hb connectivity peaks ($t > 3.5$) in similar locations along the medial brainstem were identified as dorsal, median, and magnus raphe nuclei. **P**—**Q**: Hb connectivity with the VTA and PAG remained significant ($p_{TFCE\text{-}FWE} < 0.05$) even in a secondary analysis without spatial smoothing (additional results presented in Inline Supplementary Fig. S4). **R**: Detail of Hb connectivity with the left anterior insula, posterior insula, and sensory regions of the operculum. **S**—**T**: Unthresholded negative Hb connectivity with the bilateral amygdala and inferior hippocampus.

3.3.7. *Hippocampus and amygdala*

We found significant positive Hb connectivity with superior portions of the bilateral hippocampus (Fig. 4J) and presubiculum (Fig. 4B–C), part of the parahippocampal formation. By contrast, and unlike almost every other part of the subcortex, unthresholded maps revealed weakly negative voxelwise Hb connectivity with the amygdala and inferior hippocampus (Fig. 4S–T). In the secondary parcellated analysis (Inline Supplementary Fig. S5 and Inline Supplementary Table S1), averaging the timeseries of all bilateral amygdala voxels resulted in significant negative Hb connectivity ($t = -3.6$); Hb connectivity with the mean hippocampal timeseries remained non-significant ($t = -0.81$).

3.3.8. *Sensory and motor cortices*

We observed a specific pattern of functional connectivity between the Hb and early sensory cortices. This was most conspicuous in the visual system, with significant positive connectivity cleanly segregating along the areal boundaries of the primary visual cortex (Fig. 4B–C), ringed by significant negative connectivity with the surrounding extrastriate visual cortex (Fig. 4D, right hemisphere). Unthresholded statistical maps revealed an extremely similar pattern of negative Hb connectivity with the left extrastriate visual cortex (Fig. 5C, dark borders). The secondary parcellated analysis (Inline Supplementary Fig. S5 and Inline Supplementary Table S1) also identified significant negative Hb connectivity with the mean bilateral timeseries of several extrastriate cortical parcels.

We found an analogous pattern in the auditory system: the early auditory cortex exhibited significant positive Hb connectivity bilaterally (Fig. 4A,D,R), flanked by significant negative Hb connectivity with adjacent auditory association regions in the left hemisphere (Fig. 4A). As in the visual system, negative Hb connectivity with higher auditory areas appeared symmetric in unthresholded statistical maps (Fig. 5D, dark borders).

While not explicitly mapped by the HCP sensory task paradigms, occipital regions likely corresponding to the primary gustatory cortex (area 43) and olfactory piriform cortex (area Pir) also had significant positive connectivity with the Hb (Fig. 4R).

Distinct from the other sensory systems, primary somatosensory and motor cortices showed a mix of significant positive (Fig. 4A–D) and subthreshold negative (Fig. 5E) Hb connectivity. This pattern corresponded closely with the topographic organization of the somatomotor strip: while Hb connectivity varied within the major areal divisions of the primary somatosensory and motor cortices (Fig. 5E, light borders in left panel), it segregated cleanly between somatotopic subregional boundaries (Fig. 5E, light borders in right panel). Viewed in this way, significant positive Hb connectivity encompassed portions of the somatomotor strip corresponding to the lower limbs, trunk, and eyes, while subregions corresponding to the upper limbs and face demonstrated subthreshold

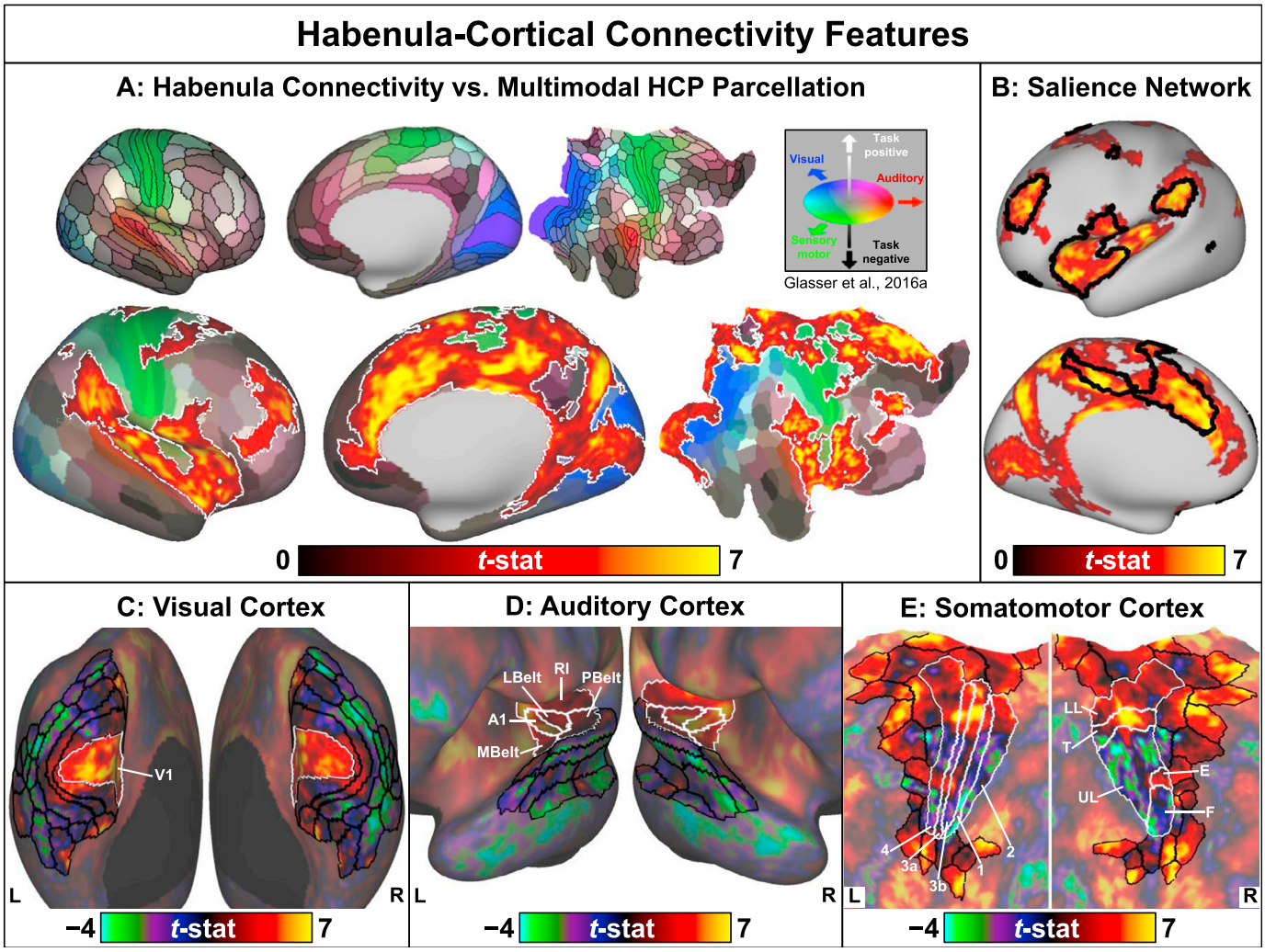

Fig. 5. Key features of Hb connectivity with the cortex. **A, Top**: Composite sensory and task responsiveness map from the multimodal HCP cortical parcellation (Glasser et al., 2016a), displayed on "very inflated" and "flat" right cortical surfaces with areal boundaries. Colors indicate association with major sensory modalities assessed by HCP tasks (blue = visual, red = auditory, green = somatosensory). Shading indicates overall responsiveness to HCP tasks (light = task-positive, dark = task-negative). **A, Bottom**: Map of significant ($p_{TFCE\text{-}FWE} < 0.05$) positive Hb connectivity (outlined in white) overlaid on the multimodal HCP parcellation. Cortical Hb connectivity included early processing areas of all major sensory modalities and was restricted to task-positive regions, terminating abruptly at boundaries with task-negative areas (e.g., dmPFC and posterior cingulate). **B**: Significant ($p_{TFCE\text{-}FWE} < 0.05$) positive Hb connectivity included nearly every part of the cortical Salience Network (outlined in black). Salience Network boundaries were created by combining networks 7 and 8 from the 17-network rs-fMRI parcellation published by Yeo et al. (2011) and distributed by the HCP. Displayed on the "very inflated" left cortical surface. **C–E**: Unthresholded Hb connectivity maps with left and right visual, auditory, and somatomotor cortices. Areal and subareal boundary lines indicate early sensory cortices (white borders) and higher sensory processing areas (black borders), as identified in the multimodal HCP parcellation. Areas outside the relevant sensory cortices are displayed at 50% saturation. **C**: Hb connectivity transitioned from positive with the primary visual cortex (area V1) to negative for the adjacent extrastriate visual cortex. Displayed on "very inflated" cortical surfaces. **D**: Similarly, Hb connectivity transitioned from positive with the early auditory cortex (areas A1, RI, LBelt, MBelt, and PBelt) to negative for adjacent auditory association areas. Displayed on "inflated" cortical surfaces. **E, Left**: By contrast, Hb connectivity varied between positive and negative within the major areal boundaries of the primary somatomotor cortex (areas 1, 2, 3a, 3b, and 4). **E, Right**: Instead, these transitions mirrored boundaries between somatotopic subregions corresponding to the lower limbs (LL), trunk (T), upper limbs (UL), eyes (E), and face (F). Unlike the visual and auditory systems, Hb connectivity was also positive with most higher somatosensory processing and motor planning areas. Displayed on "flat" cortical surfaces.

negative Hb connectivity. In further contrast to the visual and auditory systems, positive Hb connectivity extended to many higher-level somatosensory and motor regions (Fig. 4A–D and Fig. 5E, dark borders), including the parietal somatosensory association cortex, frontal eye fields (FEF), and supplementary motor area (SMA), as well as the insula (Fig. 4R), which plays a central role in interoception and awareness of internal bodily states (Mai and Paxinos, 2012).

3.4. Habenula connectivity with distributed networks

3.4.1. Reward system

Many areas involved in reward processing had significant positive Hb connectivity in our study, including the ACC, posterior orbital frontal cortex (OFC), NAc, dorsal striatum, pallidum, VTA, and raphe nuclei (Fig. 4B–C,E-K). In our secondary parcellated analysis (Inline Supplementary Fig. S5 and Inline Supplementary Table S1), significant positive Hb connectivity extended to several additional regions of the lateral OFC (areas 11l and 13l).

3.4.2. Salience Network

Whole-brain Hb connectivity also encompassed much of the "Salience Network", a set of brain regions involved in evaluating the relevance of sensory stimuli and directing attention toward those deemed to be most immediately important (Seeley et al., 2007). Fig. 5B shows the overlap

between our Hb connectivity results and cortical Salience Network areas, which center around the dorsal ACC and anterior insula but also include the medial dlPFC, medial SMA, FEF, and supramarginal gyrus (Seeley et al., 2007; Yeo et al., 2011). Many subcortical structures with significant Hb connectivity in our study (Fig. 4E–K) are also associated with the Salience Network, including the ventral striatum, dorsomedial thalamus, VTA, SN, PAG, and cerebellar lobules VI and VIIb (Seeley et al., 2007; Buckner et al., 2011).

3.4.3. Pain Matrix

In healthy adults, noxious stimuli consistently activate a "Pain Matrix" comprising the anterior and posterior insula, dorsal ACC, superior mid-cingulate, PAG, and ventrolateral thalamus (Wager et al., 2013) – all regions found to have significant positive Hb connectivity in this study. The Pain Matrix is closely related to the Salience Network, reflecting the high salience of painful stimuli (Borsook et al., 2013), but is more specifically associated with the response to noxious stimuli and includes additional posterior insula and mid-cingulate regions (Legrain et al., 2011; Kragel et al., 2018).

3.4.4. Default Mode Network

Finally, we found that significant positive Hb connectivity was restricted almost exclusively to cortical areas characterized as "task-positive" (i.e., more active during tasks than rest) in the multimodal parcellation recently released by the HCP (Glasser et al., 2016a). As illustrated in Fig. 5A, Hb connectivity fell off sharply at numerous boundaries between task-positive (light) and task-negative (dark) cortical parcels. This can be seen clearly along the anterior boundary of the ACC: significant positive Hb connectivity was tightly restricted to the dorsal ACC and a few relatively task-positive parcels in the ventral ACC (e.g., area p32), but terminated abruptly at the border of task-negative parcels in the dorsomedial prefrontal cortex (dmPFC) and ventromedial prefrontal cortex (vmPFC). By contrast, we observed significant negative Hb connectivity with the lateral temporal cortices extending into the temporal poles (Fig. 4A,D), areas that were strongly task-negative in the multimodal HCP parcellation (Fig. 5A). Unthresholded maps further revealed weakly negative Hb connectivity with the dmPFC, vmPFC, and posterior cingulate (Fig. 3, left), core regions of the task-negative "Default Mode Network". This pattern also held for the cerebellum: Hb connectivity was positive with many cerebellar areas linked to task-positive brain networks, but was non-significant and weakly negative with posterior lobules crus I and crus II, which are associated with the Default Mode Network (Buckner et al., 2011). Negative Hb connectivity with the Default Mode Network was more prominent in several of our secondary analyses. In particular, the parcellated analysis (Inline Supplementary Fig. S5 and Inline Supplementary Table S1) found significant negative Hb connectivity with parcels in the dmPFC (area 8BL) and vmPFC (area 10v), while the secondary analysis that included MGR (Inline Supplementary Fig. S3) found significant negative Hb connectivity throughout the dmPFC, vmPFC, posterior lateral parietal cortex, and right posterior cingulate.

4. Discussion

This study combined high-quality MRI data, thorough denoising procedures, rigorous inter-subject cortical alignment, and optimized ROI definitions to comprehensively assess the whole-brain functional connectivity of the human Hb. As expected, we observed robust Hb connectivity with the VTA, SN, and raphe nuclei, mirroring the close functional relationship between these structures seen across species (Boulos et al., 2017; Fore et al., 2018). Our findings of Hb connectivity with the reward (Boulos et al., 2017), pain (Shelton et al., 2012a), and motor (Hikosaka, 2010) systems are likewise highly consistent with the animal literature, suggesting that Hb function has been largely conserved through human evolution. As is typical of resting-state functional connectivity studies (Honey et al., 2009), we identified significant associations with many direct Hb afferents and efferents, but also with functionally related areas beyond established anatomical pathways. Our results highlight the benefits of cortical surface analysis (Coalson et al., 2018) to clarify such functional relationships: we found strong evidence of positive functional connectivity between the Hb and the Salience Network, while the rapid drop in Hb connectivity along task-negative cortical parcel boundaries was not apparent in our earlier, 3D volume-based fMRI study (Ely et al., 2016). Our evaluation of multiple ways to define Hb seed ROIs also sheds light on the inconsistencies in previous human Hb functional connectivity literature: while unthresholded connectivity patterns were similar across ROI types (Fig. 3, left), sensitivity to Hb BOLD signals varied dramatically (Table 1), which in turn influenced which results survived statistical thresholding (Fig. 3, right).

As in the Results, discussion of our Hb connectivity findings is broadly divided into specific brain structures (section 4.1) and distributed brain networks (section 4.2).

4.1. Habenula connectivity with specific structures

4.1.1. Ventral tegmental area and substantia nigra

Lateral Hb regulation of the dopaminergic midbrain is exceptionally well characterized in mammals (Zahm and Root, 2017), with cytological and tract-tracing studies reporting extensive lateral Hb projections via the fasciculus retroflexus to the VTA and SN (Herkenham and Nauta, 1979; Quina et al., 2015). The pattern of these projections is complex and predominantly polysynaptic: lateral Hb signaling is primarily glutamatergic, causing indirect inhibition of midbrain dopamine neurons through GABAergic interneurons in the VTA and recently recognized rostromedial tegmental nucleus (RMTg), also called the tail of the VTA (Jhou et al., 2009; Zahm and Root, 2017). A minority of lateral Hb outputs to the VTA, meanwhile, form monosynaptic excitatory synapses with dopaminergic neurons (Brown and Shepard, 2016). Interestingly, *in vivo* rs-fMRI studies in humans have consistently reported positive functional connectivity between the Hb and VTA (Ely et al., 2016; Hétu et al., 2016; Torrisi et al., 2017), suggesting that the various negative and positive feedback loops formed by these structures (Stamatakis and Stuber, 2012; Zahm and Root, 2017) result in tightly correlated low-frequency fluctuations in aggregate activity.

Like the neighboring VTA, a wealth of animal data indicate that dopaminergic cells of the SN pars compacta receive indirect inhibitory signals from the lateral Hb by way of the RMTg to suppress reward- and motor-related dopamine release (Matsumoto and Hikosaka, 2007; Jhou et al., 2009). Our finding of weaker and less spatially specific Hb-SN than Hb-VTA connectivity (Fig. 4H) likely relates to the high iron content of SN neurons (Ward et al., 2014), which resulted in non-optimal sensitivity to SN BOLD signals in the 3 T HCP fMRI acquisitions. Supporting this interpretation, previous high-resolution 3 T fMRI studies have also reported more limited Hb connectivity with the SN than VTA at rest (Ely et al., 2016; Hétu et al., 2016) and during an aversive processing task (Hennigan et al., 2015), while the only published Hb rs-fMRI study at 7 T, where SN BOLD sensitivity is even less optimal, did not detect functional connectivity with the SN (Torrisi et al., 2017).

4.1.2. Raphe nuclei

Our finding of significant Hb connectivity with the serotonergic dorsal, median, and magnus raphe nuclei (Fig. 4L–O) extends our previous, tentative identification of Hb resting-state functional connectivity with the dorsal raphe nucleus (Ely et al., 2016), which has also been reported at 7 T (Torrisi et al., 2017). In rodents, tracer studies indicate that the largest fraction of descending monosynaptic lateral Hb projections terminate in or near the dorsal and median raphe nuclei (Herkenham and Nauta, 1979; Quina et al., 2015). Similar to the dopaminergic VTA, serotonergic dorsal raphe activity is suppressed by electrical stimulation of the lateral Hb and increased by lateral Hb inhibition or lesions, although the mechanism is less well understood

(Metzger et al., 2017). Additionally, animal data indicate that both the lateral Hb (Gelegen et al., 2018) and dorsal raphe nucleus (Cho et al., 2017) play important roles in arousal and sleep-wake cycles. Projections from the dorsal, median, and especially magnus raphe nuclei to nociceptive spinal cord dorsal horn neurons are also pivotal to descending pain modulation (Griffith and Gatipon, 1981; Wang and Nakai, 1994); in part due to its influence over raphe nuclei signaling, the Hb is hence strongly implicated in the descending pain modulatory system as well (also see below).

4.1.3. Periaqueductal gray

The PAG is a key hub of the descending pain modulatory system where regulatory cortical signals and nociceptive spinal inputs converge; other important functions of the PAG include homeostatic regulation and stress response (Mai and Paxinos, 2012). The PAG receives monosynaptic projections from the lateral Hb (Ma et al., 1992) and modulates pain processing through both direct projections to the spinal cord and relays in the inferior brainstem, most prominently the magnus raphe nucleus and rostral ventromedial medulla (Mai and Paxinos, 2012). Although we did not detect significant Hb connectivity with the PAG in our previous study (Ely et al., 2016), possibly due to differences in data processing or sample composition, convergent lines of evidence strongly support a biological basis for human Hb-PAG functional connectivity. These include: (i) the consistent connectivity we observed with the PAG across Hb seed ROIs evaluated in the current study (Fig. 3), (ii) similar findings of Hb-PAG connectivity in other high-resolution rs-fMRI studies (Hétu et al., 2016; Torrisi et al., 2017), and (iii) the prominent Hb-PAG connections reported in rodent tracer experiments (Herkenham and Nauta, 1979; Quina et al., 2015).

4.1.4. Striatum

The dorsal and ventral striatum receive distinct dopaminergic inputs from the SN (nigrostriatal pathway) and VTA (mesolimbic pathway), respectively (Mai and Paxinos, 2012). In rodents, both motor-related nigrostriatal signaling and reward-related mesolimbic signaling are tightly controlled by lateral Hb inputs to the RMTg (Jhou et al., 2009). Our finding of highly significant Hb-VTA connectivity (Fig. 4H) but only moderate Hb-NAc connectivity (Fig. 4I) appears to mirror this underlying polysynaptic circuit. While previous high-resolution rs-fMRI studies have described limited Hb-striatal connectivity, which was restricted to the putamen tail and only observed at 7 T (Torrisi et al., 2017), task fMRI studies report that both painful stimuli and cues predicting them elicit increased Hb connectivity with the putamen (Shelton et al., 2012b; Hennigan et al., 2015). One study has also used anticorrelations with the putamen during a reward task as a functional localizer to help identify Hb voxels (Salas et al., 2010). Our finding of significant positive Hb connectivity with the pallidum is also notable in light of the extensive projections from the entopeduncular nucleus (homologous to the human globus pallidus internal segment) and ventral pallidum (i.e., ventral portion of the globus pallidus external segment) to the lateral Hb described in animal literature (Herkenham and Nauta, 1977), with populations of neurons in both structures transmitting reward- and aversion-related information to the Hb (Zahm and Root, 2017). As with the SN, the ability to resolve pallidal BOLD signals is limited due to iron accumulation (Ward et al., 2014), likely explaining the relatively weak Hb-pallidum connectivity observed in the current study and lack of significant pallidal findings in previous Hb resting-state functional connectivity studies (Ely et al., 2016; Hétu et al., 2016; Torrisi et al., 2017).

4.1.5. Thalamus

Studies in many non-mammalian species report direct projections from the thalamus, particularly sensory relay nuclei, to the Hb (Zahm and Root, 2017; Fore et al., 2018). Although evidence of such monosynaptic inputs is more limited in mammals, the Hb receives numerous indirect inputs from the thalamus, including the dorsomedial nucleus via the ventral pallidum and ventrolateral nucleus via the globus pallidus internal segment (Zahm and Root, 2017), while thalamic sensory relays are a major target of brainstem monoamine systems (Lőrincz and Adamantidis, 2017). In contrast to the consistent finding of positive Hb-thalamus resting-state functional connectivity (Ely et al., 2016; Hétu et al., 2016; Torrisi et al., 2017), high-resolution task fMRI studies report differential activation of the Hb and dorsomedial thalamus to negatively valenced cues (Lawson et al. 2014, 2017), suggesting a more similar tonic (i.e., resting-state) than phasic (i.e., task-based) activity profile for these adjacent structures in humans. Some of the apparent functional coupling between the Hb and thalamus observed at rest likely also reflects their similar roles as hubs linking multiple sensory, motor, and cognitive modalities across brain networks (Hikosaka, 2010).

4.1.6. Cerebellum

Our finding of extensive positive Hb connectivity with the cerebellum is somewhat surprising in light of tracer studies in rodents, which indicate an absence of monosynaptic projections between the lateral Hb and cerebellum (Herkenham and Nauta, 1979; Quina et al., 2015). One possible interpretation is that we are observing indirect connections by way of the VTA. Projections from dopaminergic VTA neurons to the cerebellum have been reported in rodents (Ikai et al., 1994), although these are largely confined to lobules crus I and crus II, regions where we observed subthreshold negative Hb connectivity. In our previous study, significant positive Hb connectivity with the cerebellum was limited to a small region of the medial inferior vermis (Ely et al., 2016). Other high-resolution Hb fMRI studies to date have unfortunately excluded the cerebellum due to limited brain coverage, although one group has reported Hb-cerebellum coactivation during the early phase of pain response at conventional fMRI resolution (Shelton et al., 2012b). As with the thalamus, it is also possible that apparent Hb connectivity with the cerebellum is a result of similar functional roles as points of convergence between diverse sensorimotor and cognitive processes, rather than direct anatomical links *per se*.

4.1.7. Hippocampus and amygdala

We observed differential Hb connectivity along the superior-inferior axis of the hippocampus, possibly reflecting functional subdivisions within the hippocampal formation. In particular, positive Hb connectivity with the superior hippocampus echoes reported lateral Hb modulation of spatial memory processing in the rodent dorsal hippocampus (Goutagny et al., 2013), possibly through serotonin-mediated potentiation of CA1 pyramidal neurons (Ferraro et al., 1997). Our results also agree with past human rs-fMRI studies, which have reported significant positive Hb connectivity with more superior/posterior portions of the hippocampus and parahippocampus (Ely et al., 2016; Torrisi et al., 2017); one study also found significant negative connectivity between the left Hb and a region of the inferior/anterior parahippocampus (Hétu et al., 2016).

Previous high-resolution Hb rs-fMRI work did not report significant connectivity with the human amygdala at 3 T (Ely et al., 2016) or 7 T (Torrisi et al., 2017); as noted by Torrisi et al., this null result is consistent with the lack of known monosynaptic Hb-amygdala projections in rodents (Herkenham and Nauta, 1979; Quina et al., 2015). In the current study, negative connectivity between the Hb and amygdala was only significant in the secondary parcellated analysis after averaging rs-fMRI signals within the entire bilateral amygdala, suggesting that our main analysis and previous studies were underpowered to detect this relatively weak anticorrelation. Interestingly, however, the amygdala was one of the few regions where we observed significantly more negative Hb connectivity in healthy adults with high, relative to low, subclinical depression scores in our prior study (Ely et al., 2016). One high-resolution task fMRI study has also reported increased connectivity between the Hb and amygdala as a function of cues predicting increasingly aversive outcomes (Lawson et al., 2014).

4.1.8. Sensory and motor cortices

Our results help clarify the nature of sensory inputs to the human Hb,

suggesting a functional link with the earliest parts of the visual and auditory systems that rapidly drops off as information propagates through higher sensory processing areas. These finding replicate and extend our previous of description of negative Hb connectivity with the right extrastriate visual cortex at 3 T (Ely et al., 2016), as well as positive Hb connectivity with several moderately sized clusters in the left primary visual and auditory cortices reported at 7 T (Torrisi et al., 2017). The preferential connectivity with primitive sensory cortices may reflect the fact that the Hb is both highly conserved through evolution (Fore et al., 2018) and emerges early in human fetal development (Nieuwenhuys et al., 2008). Our results also confirm the extensive Hb connectivity with cortical somatosensory and motor regions found in our prior 3 T rs-fMRI study (Ely et al., 2016), which included a large cluster of positive Hb connectivity with the medial somatomotor strip, approximately corresponding to the peak in the lower limb and trunk subregions of areas 3a, 3b, and 4 in the current analysis (Fig. 5E and Inline Supplementary Table S1), as well as several clusters of positive Hb connectivity along the medial SMA bordering the mid-cingulate cortex, similar to the inferior SMA and superior mid-cingulate Hb connectivity pattern seen in Fig. 4B–C. Results from our secondary analyses indicate that the ability to detect Hb connectivity with the sensory and motor cortices is strongly influenced by methodological choices, particularly how the Hb seed ROI is defined (Fig. 3) and whether MGR is performed (Inline Supplementary Fig. S3).

Although animal models indicate that Hb neurons are responsive to light and other sensory stimuli, the underlying pathways are not well characterized in mammals (Fore et al., 2018). One recent study described medial septum projections to the lateral Hb that encoded the negative valence of both auditory and somatosensory stimuli in mice, suggesting the presence of a common multisensory aversion pathway (Zhang et al., 2018). Consistent with the more extensive Hb connectivity we observed with somatomotor areas, motor suppression has been proposed as a common outcome linking diverse Hb functions (Hikosaka, 2010). For example, blocking lateral Hb outputs interferes with propofol-induced sedation in rodents, while stimulating the lateral Hb suppresses movement (Gelegen et al., 2018), specifically by reducing motivation to exert effort (Proulx et al., 2018). As in reward inhibition, these effects are largely mediated by the RMTg (Jhou et al., 2009). We therefore speculate that the human Hb receives early, low-latency inputs from all sensory modalities, but only maintains higher-level interactions with the somatosensory and motor systems.

4.2. Habenula connectivity with distributed networks

4.2.1. Reward system

As discussed above, significant Hb connectivity included the VTA and SN (Fig. 4H), dopaminergic structures that encode primary reward response, as well as the NAc and dorsal striatum (Fig. 4F,I–K), major targets of dopaminergic innervation involved in propagating reward signals to downstream cortical areas (Mai and Paxinos, 2012). Cortical Hb connectivity prominently included the ACC, replicating findings from our previous 3 T rs-fMRI study (Ely et al., 2016) and an independent study at 7 T (Torrisi et al., 2017). Among diverse functions, the ACC plays a central role in evaluating reward prediction errors (Wallis and Kennerley, 2011), a major functionality shared by the lateral Hb (Hikosaka, 2010). Indeed, simultaneous neural recordings in non-human primates indicate that the lateral Hb and ACC encode complementary information about negative reward prediction errors: lateral Hb neurons respond rapidly to negative outcomes, while ACC neurons retain information across multiple trials and predict subsequent behavioral shifts (Kawai et al., 2015). Relative to previous studies (Ely et al., 2016; Torrisi et al., 2017), Hb connectivity with the dorsal ACC was more widespread in the current analysis, presumably reflecting sensitivity gains following our Hb ROI optimization (Fig. 3) and cortical surface-based analysis (Coalson et al., 2018). Finally, we observed significant positive Hb connectivity with the left posterior OFC (Fig. 4B). The OFC plays a key role in the primate reward valuation system and is frequently reported in reward-related task fMRI studies (Wallis and Kennerley, 2011), but suffers from substantial susceptibility-induced signal dropout in typical rs-fMRI acquisitions, including the HCP (Smith et al., 2013), which made vertexwise Hb-OFC connectivity difficult to detect in our main analysis. We observed further positive Hb connectivity with the lateral OFC in our secondary parcellated analysis (Inline Supplementary Fig. S5 and Inline Supplementary Table S1), which achieved higher sensitivity by averaging timeseries from multiple vertices within each cortical parcel (see section S3.2 of Supplementary Discussion).

4.2.2. Salience Network

In our previous study, we reported significant Hb connectivity with the majority of the Salience Network, but notably not the anterior insula (Ely et al., 2016). However, that study included only subjects from the HCP with very high or low subclinical depression scores, and the anterior insula was one of the few regions to differ in Hb connectivity between these subgroups. Using a larger and more representative sample of healthy HCP subjects, we now observe a similar degree of Hb connectivity with the anterior insula and dorsal ACC, in line with the tight functional coupling between these cortical areas observed during rest, salience evaluation, error monitoring, and pain response (Seeley et al., 2007; Medford and Critchley, 2010). Moreover, significant Hb connectivity with the Salience Network captured a number of relatively subtle features. For example, we only observed Hb connectivity with area PSL of the temporoparietal junction (TPJ) in the right hemisphere (arrow in Fig. 4D), mirroring reports of lateralized right TPJ connectivity with other Salience Network areas (Kucyi et al., 2012). Our detection of Hb connectivity with area IP2 of the lateral intraparietal cortex (arrow in Fig. 4A) is also noteworthy: although not generally ascribed to the Salience Network in rs-fMRI network parcellations (Yeo et al., 2011), area IP2 neurons are described as having a “pure salience response” in monkeys, preferentially firing in response to meaningful vs. distracting stimuli (Arcizet et al., 2011). As such, the Hb appears to be specifically linked with diverse cortical regions involved in salience processing.

Recent rs-fMRI work has revealed a close relationship between the Salience Network and the dopamine system. Several studies have reported functional connectivity with the dorsal ACC and anterior insula using seeds in the midbrain and brainstem, including the VTA and SN (Murty et al., 2014; Bär et al., 2016). Furthermore, acute reductions in dopamine synthesis capacity disproportionately destabilize the Salience and Somatomotor Networks (Shafiei et al., 2018), while a hybrid positron emission tomography (PET)/fMRI study found that dopamine synthesis and release capacities influence connectivity of the Salience Network but not other major networks (McCutcheon et al., 2018). Though first characterized in humans, homologous networks have since been described in non-human primates (Touroutoglou et al., 2016) and rodents (Sforazzini et al., 2014), indicating that the Salience Network is a conserved feature of large-scale brain organization in mammals. In mice, stimulating or inhibiting dopaminergic cells within the dorsal raphe nucleus respectively promotes or impairs wakefulness in response to salient stimuli (Cho et al., 2017), while retrograde labeling injections into the rat lateral Hb tag cells in both the anterior insula and ACC (Zahm and Root, 2017). Given the proposed role of the Hb in modifying behavior to avoid adverse outcomes (Hikosaka, 2010), a close functional relationship with the Salience Network is highly plausible.

4.2.3. Pain Matrix

A few of small-scale human neuroimaging studies have previously linked the Hb to both acute and chronic pain, respectively assessed by task fMRI and rs-fMRI. For acute pain, noxious heat stimulation induced rapid and sustained increases in bilateral Hb activity in healthy adults (Shelton et al., 2012b). For chronic pain, pediatric patients with chronic regional pain syndrome relative to healthy controls showed increased Hb resting-state functional connectivity with the dorsal ACC, but reduced Hb connectivity with the medial SMA, medial primary motor cortex, lateral

premotor cortex, and dlPFC (Erpelding et al., 2014). While these are the only published studies to date that explicitly examined the Hb in the context of pain, it is worth noting that several high-resolution task fMRI studies have reported significant Hb activation in response to cues predicting painful electric shocks (Lawson et al., 2014; Hennigan et al., 2015). Animal studies indicate that the Hb receives nociceptive signals both directly, via projections from the spinal cord, and indirectly, through the lateral hypothalamus (Shelton et al., 2012a). In rats, noxious formalin injections were found to stimulate high-frequency firing in a subset of lateral Hb neurons; this effect was potentiated in a chronic unpredictable stress model of depression but ameliorated by systemic antidepressant injections (Li et al., 2016). Moreover, both morphine injections and electrical stimulation targeting the Hb produce analgesia (Shelton et al., 2012a; Boulos et al., 2017). Our results thus add to converging lines of evidence placing the human Hb within the broader Pain Matrix.

4.2.4. Default Mode Network

Although we previously reported positive Hb connectivity with a handful of task-negative Default Mode Network areas using 3D volume-based fMRI analysis (Ely et al., 2016), more accurate 2D surface-based analysis now indicates that positive Hb connectivity is strongly biased toward task-positive brain regions (Fig. 5A). The few Default Mode Network areas with significant positive Hb connectivity were parts of the ventral ACC (areas p32 and a24) and mid-/posterior cingulate (areas 23d and 31a) that were characterized as relatively task-positive in the multimodal HCP parcellation (Glasser et al., 2016a), indicating that they are involved in externally as well as internally oriented mental processes. Hb connectivity was otherwise weakly negative throughout the Default Mode Network in our main analysis; this pattern was more significant in a secondary analysis that included MGR (Inline Supplementary Fig. S3), which tends to strengthen anticorrelations in rs-fMRI data (see section S3.2 of Supplementary Discussion). The systematic bias in Hb connectivity toward task-positive brain regions contrasts with the VTA and raphe nuclei, which showed positive functional connectivity with both the Default Mode and Salience Networks in a recent high-resolution brainstem rs-fMRI study (Bär et al., 2016). Instead, our results suggest that the Hb preferentially interfaces with brain regions that are engaged by externally oriented activities.

4.3. Limitations and future directions

One limitation of the current study is the difficulty of accurately localizing BOLD signals from small anatomical structures and functional subdivisions within the brainstem (Bär et al., 2016). Although Hb connectivity was significant throughout much of the midbrain and pons, we have therefore restricted our discussion to structures we could confidently identify based on probabilistic atlases and anatomical landmarks (i.e., VTA, SN, raphe nuclei, and PAG). As the RMTg has yet to be characterized in humans, we were also unable to explicitly assess its functional connectivity with the Hb. Despite the high resolution of HCP rs-fMRI data, it was likewise not feasible to distinguish BOLD signals from the lateral and medial Hb due to their small sizes. However, the lateral nucleus comprises more than 90% of the human Hb (Ahumada-Galleguillos et al., 2017), implying that our analyses predominantly measured lateral Hb connectivity.

The HCP's high-resolution imaging approach was largely motivated by the desire to accurately map functional data and areal parcels on the cortical surface (Glasser et al., 2016b). Although surface-based fMRI analysis has many benefits, it imposes a distinction in the way data in the cortex and subcortex are treated. In particular, the resampling of natively voxelwise fMRI data to the cortical ribbon effectively acts as a type of spatial smoothing (see section S3.2 of Supplementary Discussion), and means that results must be computed and visualized separately for cortical surfaces and subcortical volumes. The lack of commonly agreed upon coordinates for reporting cortical findings is also a potential concern for future meta-analyses, although spherical coordinate systems have been proposed (Fischl et al., 1999; Van Essen et al., 2001). For this study, we chose to report significant Hb connectivity with a standard set of cortical parcels in Table S1, and have made all results publicly available via the BALSA database (Van Essen et al., 2017).

The high spatial and temporal resolution of HCP rs-fMRI acquisitions also resulted in reduced voxelwise temporal signal-to-noise ratios (SNR), particularly for subcortical voxels (Smith et al., 2013), due to the high multiband factor and concomitant noise amplification and aliasing (Xu et al., 2013). Although data quality was improved by our denoising procedures (Inline Supplementary Fig. S1), residual artifacts due to interactions between head motion, physiological noise, and multiband aliasing were likely still present (Burgess et al., 2016). These factors may account for the relatively low effect size of our Hb connectivity results, as indexed by correlation strengths in the Hb-VTA ROI analysis (Table 1) and secondary parcellated analysis (Table S1). The high statistical significance of these correlations partially reflects the large number of timepoints included in each four-run average; calculating Hb-VTA connectivity for each run separately yielded similar mean correlation strengths but higher inter-subject variances and correspondingly lower significance values (section 3.3.1). Nevertheless, sensitivity and reliability of functional connectivity measurements are generally improved by higher sample rates and longer scan durations (Birn et al., 2013), while the reduced voxelwise SNR of high-resolution HCP rs-fMRI data was counterbalanced by the improved ability to localize BOLD signals, enabling us to create *Shape Optimized* ROIs that captured subject-level variations in Hb anatomy and significantly improved Hb BOLD sensitivity (see section S3.1 of Supplementary Discussion for additional considerations related to creating and evaluating Hb seed ROIs). We therefore urge future Hb fMRI studies to prioritize high-resolution acquisitions, high-quality anatomical segmentation, high-sensitivity functional ROIs, and high-fidelity surface-based analyses.

5. Conclusions

Research in small animals and nonhuman primates has increasingly implicated the Hb in a range of mental illnesses, particularly depression and addiction. Translating these preclinical discoveries to benefit people with psychiatric or substance abuse disorders will require better tools to accurately measure *in vivo* Hb activity and a better understanding of human Hb function. In this study, we developed neuroanatomically informed analysis techniques to map the resting-state functional connectivity of the human Hb in unprecedented detail using high-resolution fMRI data from healthy young adults. Our approach included an optimized strategy for extracting Hb BOLD signals as well as multimodal surface alignment and surface-based analysis for enhanced cortical sensitivity. Our results confirm the conserved nature of human Hb connectivity with key dopaminergic and serotonergic targets while replicating and extending the close functional relationships with reward system, Salience Network, Pain Matrix, and sensorimotor areas described in previous high-resolution rs-fMRI studies. We further detected a previously unappreciated bias in Hb connectivity, which strongly favored task-positive brain areas and decreased rapidly near boundaries with the task-negative Default Mode Network.

In addition to advancing our knowledge of human Hb circuitry and refining methodology for Hb fMRI studies, the current study provides a much-needed guidepost for ongoing human Hb research. For example, our finding of highly specific Hb connectivity with the early visual cortex dovetails with a very recent report of unexpected human Hb deactivation in response to changes in luminance at both 3 T and 7 T (Kaiser et al., 2019). These complementary results highlight the potential of functional connectivity patterns to guide and corroborate task fMRI investigations. Furthermore, an accurate map of Hb connectivity in healthy adults is critical for designing and interpreting studies of Hb function in clinical contexts, as illustrated by our previous investigation: although we found stronger Hb connectivity with the insula in subjects with low vs. high

subclinical depression scores, connectivity differences between these subgroups prevented us from detecting Hb-insula connectivity in the full sample (Ely et al., 2016), a fact that only became apparent once we completed the current study using a representative cohort of healthy young adults. Although mounting evidence implicates the Hb in psychopathology, it remains unknown at present which Hb fMRI metrics are sensitive and specific enough to reliably predict clinical outcomes; establishing a high-quality map of normative human Hb connectivity lays the groundwork for evaluating and improving such metrics going forward.

Note

Preliminary findings from this study were presented at the 47th (Abstract 4181) and 48th (Abstracts 2548 and 2825) Annual Meetings of the Organization for Human Brain Mapping (OHBM) as well as the 17th World Congress on Pain (Abstract 472694) hosted by the International Association for the Study of Pain (IASP). Additionally, this manuscript is included in Benjamin Ely's doctoral dissertation, in partial fulfillment of the PhD degree requirements at Icahn School of Medicine at Mount Sinai.

Funding

This work was supported by the National Institute of Mental Health (grant numbers R33-MH107589 and R01-MH111794 to ERS, R01-MH101479 and R01-MH095807 to VG, and F31-MH109257 to BAE); the National Multiple Sclerosis Society (grant number FG-1606-24492 to J-WK); and the Brain and Behavior Research Foundation (grant number NARSAD22324 to JX).

Acknowledgements

We are grateful to Drs. Abraham Z. Snyder, Matthew F. Glasser, and David C. Van Essen at Washington University School of Medicine for discussions related to the interpretation of our results, and to Mr. Chen Yang at the Translational and Molecular Imaging Institute in the Icahn School of Medicine at Mount Sinai (ISMMS) for assistance with data management. This work was supported in part through the computational resources and staff expertise provided by ISMMS Scientific Computing, with additional resource support provided by the ISMMS Brain Imaging Center. Data were provided by the Human Connectome Project, WU-Minn Consortium (Principal Investigators: David Van Essen and Kamil Ugurbil; U54-MH091657), funded by the 16 National Institutes of Health (NIH) Institutes and Centers that support the NIH Blueprint for Neuroscience Research; and by the McDonnell Center for Systems Neuroscience at Washington University.

Appendix A. Supplementary data

Supplementary data to this article can be found online at https://doi.org/10.1016/j.neuroimage.2019.06.015.

Conflicts of interest

The authors declare no competing financial interests or other relevant conflicts.

References

Ahumada-Galleguillos, P., Lemus, C.G., Diaz, E., Osorio-Reich, M., Hartel, S., Concha, M.L., 2017. Directional asymmetry in the volume of the human habenula. Brain Struct. Funct. 222, 1087–1092.

Arcizet, F., Mirpour, K., Bisley, J.W., 2011. A pure salience response in posterior parietal cortex. Cerebr. Cortex 21, 2498–2506.

Bär, K.-J., De La Cruz, F., Schumann, A., Koehler, S., Sauer, H., Critchley, H., Wagner, G., 2016. Functional connectivity and network analysis of midbrain and brainstem nuclei. Neuroimage 134, 53–63.

Birn, R.M., Molloy, E.K., Patriat, R., Parker, T., Meier, T.B., Kirk, G.R., Nair, V.A., Meyerand, M.E., Prabhakaran, V., 2013. The effect of scan length on the reliability of resting-state fMRI connectivity estimates. Neuroimage 83, 550–558.

Borsook, D., Edwards, R., Elman, I., Becerra, L., Levine, J., 2013. Pain and analgesia: the value of salience circuits. Prog. Neurobiol. 104, 93–105.

Boulos, L.J., Darcq, E., Kieffer, B.L., 2017. Translating the habenula-from rodents to humans. Biol. Psychiatry 81, 296–305.

Brown, P.L., Shepard, P.D., 2016. Functional evidence for a direct excitatory projection from the lateral habenula to the ventral tegmental area in the rat. J. Neurophysiol. 116, 1161–1174.

Buckner, R.L., Krienen, F.M., Castellanos, A., Diaz, J.C., Yeo, B.T., 2011. The organization of the human cerebellum estimated by intrinsic functional connectivity. J. Neurophysiol. 106, 2322–2345.

Burgess, G.C., Kandala, S., Nolan, D., Laumann, T.O., Power, J.D., Adeyemo, B., Harms, M.P., Petersen, S.E., Barch, D.M., 2016. Evaluation of denoising strategies to address motion-correlated artifacts in resting-state functional magnetic resonance imaging data from the Human Connectome Project. Brain Connect. 6, 669–680.

Cho, J.R., Treweek, J.B., Robinson, J.E., Xiao, C., Bremner, L.R., Greenbaum, A., Gradinaru, V., 2017. Dorsal raphe dopamine neurons modulate arousal and promote wakefulness by salient stimuli. Neuron 94, 1205–1219 e1208.

Coalson, T.S., Van Essen, D.C., Glasser, M.F., 2018. The impact of traditional neuroimaging methods on the spatial localization of cortical areas. Proc. Natl. Acad. Sci. U.S.A. 115, E6356–E6365.

Ely, B.A., Xu, J., Goodman, W.K., Lapidus, K.A., Gabbay, V., Stern, E.R., 2016. Resting-state functional connectivity of the human habenula in healthy individuals: associations with subclinical depression. Hum. Brain Mapp. 37, 2369–2384.

Erpelding, N., Sava, S., Simons, L.E., Lebel, A., Serrano, P., Becerra, L., Borsook, D., 2014. Habenula functional resting-state connectivity in pediatric CRPS. J. Neurophysiol. 111, 239–247.

Ferraro, G., Montalbano, M.E., Sardo, P., La Grutta, V., 1997. Lateral habenula and hippocampus: a complex interaction raphe cells-mediated. J. Neural Transm. 104, 615–631.

Fischl, B., Sereno, M.I., Dale, A.M., 1999. Cortical surface-based analysis. II: inflation, flattening, and a surface-based coordinate system. Neuroimage 9, 195–207.

Fore, S., Palumbo, F., Pelgrims, R., Yaksi, E., 2018. Information processing in the vertebrate habenula. Semin. Cell Dev. Biol. 78, 130–139.

Fox, M.D., Raichle, M.E., 2007. Spontaneous fluctuations in brain activity observed with functional magnetic resonance imaging. Nat. Rev. Neurosci. 8, 700–711.

Gelegen, C., Miracca, G., Ran, M.Z., Harding, E.C., Ye, Z., Yu, X., Tossell, K., Houston, C.M., Yustos, R., Hawkins, E.D., Vyssotski, A.L., Dong, H.L., Wisden, W., Franks, N.P., 2018. Excitatory pathways from the lateral habenula enable propofol-induced sedation. Curr. Biol. 28, 580–587 e585.

Glasser, M.F., Coalson, T.S., Robinson, E.C., Hacker, C.D., Harwell, J., Yacoub, E., Ugurbil, K., Andersson, J., Beckmann, C.F., Jenkinson, M., Smith, S.M., Van Essen, D.C., 2016a. A multi-modal parcellation of human cerebral cortex. Nature 536, 171–178.

Glasser, M.F., Smith, S.M., Marcus, D.S., Andersson, J.L., Auerbach, E.J., Behrens, T.E., Coalson, T.S., Harms, M.P., Jenkinson, M., Moeller, S., Robinson, E.C., Sotiropoulos, S.N., Xu, J., Yacoub, E., Ugurbil, K., Van Essen, D.C., 2016b. The Human Connectome Project's neuroimaging approach. Nat. Neurosci. 19, 1175–1187.

Glasser, M.F., Sotiropoulos, S.N., Wilson, J.A., Coalson, T.S., Fischl, B., Andersson, J.L., Xu, J., Jbabdi, S., Webster, M., Polimeni, J.R., Van Essen, D.C., Jenkinson M for the WU-Minn HCP Consortium, 2013. The minimal preprocessing pipelines for the Human Connectome Project. Neuroimage 80, 105–124.

Goutagny, R., Loureiro, M., Jackson, J., Chaumont, J., Williams, S., Isope, P., Kelche, C., Cassel, J.C., Lecourtier, L., 2013. Interactions between the lateral habenula and the hippocampus: implication for spatial memory processes. Neuropsychopharmacology 38, 2418–2426.

Griffanti, L., Salimi-Khorshidi, G., Beckmann, C.F., Auerbach, E.J., Douaud, G., Sexton, C.E., Zsoldos, E., Ebmeier, K.P., Filippini, N., Mackay, C.E., Moeller, S., Xu, J., Yacoub, E., Baselli, G., Ugurbil, K., Miller, K.L., Smith, S.M., 2014. ICA-based artefact removal and accelerated fMRI acquisition for improved resting state network imaging. Neuroimage 95, 232–247.

Griffith, J.L., Gatipon, G.B., 1981. A comparative study of selective stimulation of raphe nuclei in the cat in inhibiting dorsal horn neuron responses to noxious stimulation. Brain Res. 229, 520–524.

Hennigan, K., D'ardenne, K., Mcclure, S.M., 2015. Distinct midbrain and habenula pathways are involved in processing aversive events in humans. J. Neurosci. 35, 198–208.

Herkenham, M., Nauta, W.J., 1977. Afferent connections of the habenular nuclei in the rat. A horseradish peroxidase study, with a note on the fiber-of-passage problem. J. Comp. Neurol. 173, 123–146.

Herkenham, M., Nauta, W.J., 1979. Efferent connections of the habenular nuclei in the rat. J. Comp. Neurol. 187, 19–47.

Hétu, S., Luo, Y., Saez, I., D'ardenne, K., Lohrenz, T., Montague, P.R., 2016. Asymmetry in functional connectivity of the human habenula revealed by high-resolution cardiac-gated resting state imaging. Hum. Brain Mapp. 37, 2602–2615.

Hikosaka, O., 2010. The habenula: from stress evasion to value-based decision-making. Nat. Rev. Neurosci. 11, 503–513.

Honey, C.J., Sporns, O., Cammoun, L., Gigandet, X., Thiran, J.P., Meuli, R., Hagmann, P., 2009. Predicting human resting-state functional connectivity from structural connectivity. Proc. Natl. Acad. Sci. U.S.A. 106, 2035–2040.

Ikai, Y., Takada, M., Mizuno, N., 1994. Single neurons in the ventral tegmental area that project to both the cerebral and cerebellar cortical areas by way of axon collaterals. Neuroscience 61, 925–934.

Jakab, A., Blanc, R., Berenyi, E.L., Szekely, G., 2012. Generation of individualized thalamus target maps by using statistical shape models and thalamocortical tractography. AJNR Am. J. Neuroradiol. 33, 2110–2116.
Jenkinson, M., Bannister, P., Brady, M., Smith, S., 2002. Improved optimization for the robust and accurate linear registration and motion correction of brain images. Neuroimage 17, 825–841.
Jhou, T.C., Fields, H.L., Baxter, M.G., Saper, C.B., Holland, P.C., 2009. The rostromedial tegmental nucleus (RMTg), a GABAergic afferent to midbrain dopamine neurons, encodes aversive stimuli and inhibits motor responses. Neuron 61, 786–800.
Kaiser, C., Kaufmann, C., Leutritz, T., Arnold, Y.L., Speck, O., Ullsperger, M., 2019. The human habenula is responsive to changes in luminance and circadian rhythm. Neuroimage 189, 581–588.
Kawai, T., Yamada, H., Sato, N., Takada, M., Matsumoto, M., 2015. Roles of the lateral habenula and anterior cingulate cortex in negative outcome monitoring and behavioral adjustment in nonhuman primates. Neuron 88, 792–804.
Kim, J.-W., Naidich, T.P., Ely, B.A., Yacoub, E., De Martino, F., Fowkes, M.E., Goodman, W.K., Xu, J., 2016. Human habenula segmentation using myelin content. Neuroimage 130, 145–156.
Kim, J.-W., Naidich, T.P., Joseph, J., Nair, D., Glasser, M.F., O'halloran, R., Doucet, G.E., Lee, W.H., Krinsky, H., Paulino, A., Glahn, D.C., Anticevic, A., Frangou, S., Xu, J., 2018. Reproducibility of myelin content-based human habenula segmentation at 3 Tesla. Hum. Brain Mapp. 39, 3058–3071.
Kragel, P.A., Kano, M., Van Oudenhove, L., Ly, H.G., Dupont, P., Rubio, A., Delon-Martin, C., Bonaz, B.L., Manuck, S.B., Gianaros, P.J., Ceko, M., Reynolds Losin, E.A., Woo, C.W., Nichols, T.E., Wager, T.D., 2018. Generalizable representations of pain, cognitive control, and negative emotion in medial frontal cortex. Nat. Neurosci. 21, 283–289.
Krauth, A., Blanc, R., Poveda, A., Jeanmonod, D., Morel, A., Szekely, G., 2010. A mean three-dimensional atlas of the human thalamus: generation from multiple histological data. Neuroimage 49, 2053–2062.
Kucyi, A., Hodaie, M., Davis, K.D., 2012. Lateralization in intrinsic functional connectivity of the temporoparietal junction with salience- and attention-related brain networks. J. Neurophysiol. 108, 3382–3392.
Lawson, R.P., Nord, C.L., Seymour, B., Thomas, D.L., Dayan, P., Pilling, S., Roiser, J.P., 2017. Disrupted habenula function in major depression. Mol. Psychiatry 22, 202–208.
Lawson, R.P., Seymour, B., Loh, E., Lutti, A., Dolan, R.J., Dayan, P., Weiskopf, N., Roiser, J.P., 2014. The habenula encodes negative motivational value associated with primary punishment in humans. Proc. Natl. Acad. Sci. U.S.A. 111, 11858–11863.
Legrain, V., Iannetti, G.D., Plaghki, L., Mouraux, A., 2011. The pain matrix reloaded: a salience detection system for the body. Prog. Neurobiol. 93, 111–124.
Li, J., Li, Y., Zhang, B., Shen, X., Zhao, H., 2016. Why depression and pain often coexist and mutually reinforce: role of the lateral habenula. Exp. Neurol. 284, 106–113.
Lőrincz, M.L., Adamantidis, A.R., 2017. Monoaminergic control of brain states and sensory processing: existing knowledge and recent insights obtained with optogenetics. Prog. Neurobiol. 151, 237–253.
Ma, Q.P., Shi, Y.S., Han, J.S., 1992. Further studies on interactions between periaqueductal gray, nucleus accumbens and habenula in antinociception. Brain Res. 583, 292–295.
Mai, J.R.K., Paxinos, G. (Eds.), 2012. The Human Nervous System, third ed. Elsevier Academic Press, Amsterdam (Netherlands).
Marcus, D.S., Harwell, J., Olsen, T., Hodge, M., Glasser, M.F., Prior, F., Jenkinson, M., Laumann, T., Curtiss, S.W., Van Essen, D.C., 2011. Informatics and data mining tools and strategies for the Human Connectome Project. Front. Neuroinf. 5, 4.
Matsumoto, M., Hikosaka, O., 2007. Lateral habenula as a source of negative reward signals in dopamine neurons. Nature 447, 1111–1115.
McCutcheon, R.A., Nour, M.M., Dahoun, T., Jauhar, S., Pepper, F., Expert, P., Veronese, M., Adams, R.A., Turkheimer, F., Mehta, M.A., Howes, O.D., 2018. Mesolimbic dopamine function is related to salience network connectivity: an integrative positron emission tomography and magnetic resonance study. Biol. Psychiatry 85, 368–378.
Medford, N., Critchley, H.D., 2010. Conjoint activity of anterior insular and anterior cingulate cortex: awareness and response. Brain Struct. Funct. 214, 535–549.
Metzger, M., Bueno, D., Lima, L.B., 2017. The lateral habenula and the serotonergic system. Pharmacol. Biochem. Behav. 162, 22–28.
Murty, V.P., Shermohammed, M., Smith, D.V., Carter, R.M., Huettel, S.A., Adcock, R.A., 2014. Resting state networks distinguish human ventral tegmental area from substantia nigra. Neuroimage 100, 580–589.
Nieuwenhuys, R., Voogd, J., Van Huijzen, C. (Eds.), 2008. The Human Central Nervous System, fourth ed. Springer, New York (NY).
Proulx, C.D., Aronson, S., Milivojevic, D., Molina, C., Loi, A., Monk, B., Shabel, S.J., Malinow, R., 2018. A neural pathway controlling motivation to exert effort. Proc. Natl. Acad. Sci. U.S.A. 115, 5792–5797.
Quina, L.A., Tempest, L., Ng, L., Harris, J.A., Ferguson, S., Jhou, T.C., Turner, E.E., 2015. Efferent pathways of the mouse lateral habenula. J. Comp. Neurol. 523, 32–60.
Robinson, E.C., Jbabdi, S., Glasser, M.F., Andersson, J., Burgess, G.C., Harms, M.P., Smith, S.M., Van Essen, D.C., Jenkinson, M., 2014. MSM: a new flexible framework for multimodal surface matching. Neuroimage 100, 414–426.
Salas, R., Baldwin, P., De Biasi, M., Montague, P.R., 2010. BOLD responses to negative reward prediction errors in human habenula. Front. Hum. Neurosci. 4, 36.
Salimi-Khorshidi, G., Douaud, G., Beckmann, C.F., Glasser, M.F., Griffanti, L., Smith, S.M., 2014. Automatic denoising of functional MRI data: combining independent component analysis and hierarchical fusion of classifiers. Neuroimage 90, 449–468.
Seeley, W.W., Menon, V., Schatzberg, A.F., Keller, J., Glover, G.H., Kenna, H., Reiss, A.L., Greicius, M.D., 2007. Dissociable intrinsic connectivity networks for salience processing and executive control. J. Neurosci. 27, 2349–2356.
Sforazzini, F., Schwarz, A.J., Galbusera, A., Bifone, A., Gozzi, A., 2014. Distributed BOLD and CBV-weighted resting-state networks in the mouse brain. Neuroimage 87, 403–415.
Shafiei, G., Zeighami, Y., Clark, C.A., Coull, J.T., Nagano-Saito, A., Leyton, M., Dagher, A., Misic, B., 2018. Dopamine signaling modulates the stability and integration of intrinsic brain networks. Cerebr. Cortex 29, 397–409.
Shelton, L., Becerra, L., Borsook, D., 2012a. Unmasking the mysteries of the habenula in pain and analgesia. Prog. Neurobiol. 96, 208–219.
Shelton, L., Pendse, G., Maleki, N., Moulton, E.A., Lebel, A., Becerra, L., Borsook, D., 2012b. Mapping pain activation and connectivity of the human habenula. J. Neurophysiol. 107, 2633–2648.
Smith, S.M., Beckmann, C.F., Andersson, J., Auerbach, E.J., Bijsterbosch, J., Douaud, G., Duff, E., Feinberg, D.A., Griffanti, L., Harms, M.P., Kelly, M., Laumann, T., Miller, K.L., Moeller, S., Petersen, S., Power, J., Salimi-Khorshidi, G., Snyder, A.Z., Vu, A.T., Woolrich, M.W., Xu, J., Yacoub, E., Ugurbil, K., Van Essen, D.C., Glasser MF for the WU-Minn HCP Consortium, 2013. Resting-state fMRI in the Human Connectome Project. Neuroimage 80, 144–168.
Son, Y.-D., Cho, Z.-H., Kim, H.-K., Choi, E.-J., Lee, S.-Y., Chi, J.-G., Park, C.-W., Kim, Y.-B., 2012. Glucose metabolism of the midline nuclei raphe in the brainstem observed by PET-MRI fusion imaging. Neuroimage 59, 1094–1097.
Stamatakis, A.M., Stuber, G.D., 2012. Activation of lateral habenula inputs to the ventral midbrain promotes behavioral avoidance. Nat. Neurosci. 15, 1105–1107.
Stamatakis, A.M., Van Swieten, M., Basiri, M.L., Blair, G.A., Kantak, P., Stuber, G.D., 2016. Lateral hypothalamic area glutamatergic neurons and their projections to the lateral habenula regulate feeding and reward. J. Neurosci. 36, 302–311.
Sutherland, R.J., 1982. The dorsal diencephalic conduction system: a review of the anatomy and functions of the habenular complex. Neurosci. Biobehav. Rev. 6, 1–13.
Torrisi, S., Nord, C.L., Balderston, N.L., Roiser, J.P., Grillon, C., Ernst, M., 2017. Resting state connectivity of the human habenula at ultra-high field. Neuroimage 147, 872–879.
Touroutoglou, A., Bliss-Moreau, E., Zhang, J., Mantini, D., Vanduffel, W., Dickerson, B.C., Barrett, L.F., 2016. A ventral salience network in the macaque brain. Neuroimage 132, 190–197.
Van Essen, D.C., Lewis, J.W., Drury, H.A., Hadjikhani, N., Tootell, R.B., Bakircioglu, M., Miller, M.I., 2001. Mapping visual cortex in monkeys and humans using surface-based atlases. Vis. Res. 41, 1359–1378.
Van Essen, D.C., Smith, J., Glasser, M.F., Elam, J., Donahue, C.J., Dierker, D.L., Reid, E.K., Coalson, T., Harwell, J., 2017. The Brain Analysis Library of Spatial maps and Atlases (BALSA) database. Neuroimage 144, 270–274.
Van Essen, D.C., Smith, S.M., Barch, D.M., Behrens, T.E., Yacoub, E., Ugurbil K for the WU-Minn HCP Consortium, 2013. The WU-Minn Human Connectome Project: an overview. Neuroimage 80, 62–79.
Wager, T.D., Atlas, L.Y., Lindquist, M.A., Roy, M., Woo, C.W., Kross, E., 2013. An fMRI-based neurologic signature of physical pain. N. Engl. J. Med. 368, 1388–1397.
Wallis, J.D., Kennerley, S.W., 2011. Contrasting reward signals in the orbitofrontal cortex and anterior cingulate cortex. Ann. NY Acad. Sci. 1239, 33–42.
Wang, Q.P., Nakai, Y., 1994. The dorsal raphe: an important nucleus in pain modulation. Brain Res. Bull. 34, 575–585.
Ward, R.J., Zucca, F.A., Duyn, J.H., Crichton, R.R., Zecca, L., 2014. The role of iron in brain ageing and neurodegenerative disorders. Lancet Neurol. 13, 1045–1060.
Whitfield-Gabrieli, S., Nieto-Castanon, A., 2012. Conn: a functional connectivity toolbox for correlated and anticorrelated brain networks. Brain Connect. 2, 125–141.
Winkler, A.M., Ridgway, G.R., Webster, M.A., Smith, S.M., Nichols, T.E., 2014. Permutation inference for the general linear model. Neuroimage 92, 381–397.
Winkler, A.M., Webster, M.A., Vidaurre, D., Nichols, T.E., Smith, S.M., 2015. Multi-level block permutation. Neuroimage 123, 253–268.
Xu, J., Moeller, S., Auerbach, E.J., Strupp, J., Smith, S.M., Feinberg, D.A., Yacoub, E., Ugurbil, K., 2013. Evaluation of slice accelerations using multiband echo planar imaging at 3 T. Neuroimage 83, 991–1001.
Yang, Y., Cui, Y., Sang, K., Dong, Y., Ni, Z., Ma, S., Hu, H., 2018. Ketamine blocks bursting in the lateral habenula to rapidly relieve depression. Nature 554, 317–322.
Yeo, B.T., Krienen, F.M., Sepulcre, J., Sabuncu, M.R., Lashkari, D., Hollinshead, M., Roffman, J.L., Smoller, J.W., Zollei, L., Polimeni, J.R., Fischl, B., Liu, H., Buckner, R.L., 2011. The organization of the human cerebral cortex estimated by intrinsic functional connectivity. J. Neurophysiol. 106, 1125–1165.
Zahm, D.S., Root, D.H., 2017. Review of the cytology and connections of the lateral habenula, an avatar of adaptive behaving. Pharmacol. Biochem. Behav. 162, 3–21.
Zapata, A., Hwang, E.K., Lupica, C.R., 2017. Lateral habenula involvement in impulsive cocaine seeking. Neuropsychopharmacology 42, 1103–1112.
Zhang, G.W., Shen, L., Zhong, W., Xiong, Y., Zhang, L.I., Tao, H.W., 2018. Transforming sensory cues into aversive emotion via septal-habenular pathway. Neuron 99, 1016–1028.